H. B. Robinson-2
Pressure Vessel Benchmark

Prepared by
I. Remec, F. B. K. Kam

Oak Ridge National Laboratory
Managed by Lockheed Martin Energy Research Corp.

Oak Ridge National Laboratory
Oak Ridge, TN 37831-6363

C. J. Fairbanks, NRC Project Manager

MASTER

DISCLAIMER

DISCLAIMER

Portions of this document may be illegible electronic image products. Images are produced from the best available original document.

ABSTRACT

The H. B. Robinson Unit 2 Pressure Vessel Benchmark (HBR-2 benchmark) is described and analyzed in this report. Analysis of the HBR-2 benchmark can be used as partial fulfillment of the requirements for the qualification of the methodology for calculating neutron fluence in pressure vessels, as required by the U.S. Nuclear Regulatory Commission Regulatory Guide DG-1053, *Calculational and Dosimetry Methods for Determining Pressure Vessel Neutron Fluence*.

Section 1 of this report describes the HBR-2 benchmark and provides all the dimensions, material compositions, and neutron source data necessary for the analysis. The measured quantities, to be compared with the calculated values, are the specific activities at the end of fuel cycle 9. The characteristic feature of the HBR-2 benchmark is that it provides measurements on both sides of the pressure vessel: in the surveillance capsule attached to the thermal shield and in the reactor cavity.

In Section 2, the analysis of the HBR-2 benchmark is described. Calculations with the computer code DORT, based on the discrete-ordinates method, were performed with three multigroup libraries based on ENDF/B-VI: BUGLE-93, SAILOR-95 and BUGLE-96. The average ratio of the calculated-to-measured specific activities (C/M) for the six dosimeters in the surveillance capsule was 0.90 ± 0.04 for all three libraries. The average C/Ms for the cavity dosimeters (without neptunium dosimeter) were 0.89 ± 0.10, 0.91 ± 0.10, and 0.90 ± 0.09 for the BUGLE-93, SAILOR-95 and BUGLE-96 libraries, respectively.

It is expected that the agreement of the calculations with the measurements, similar to the agreement obtained in this research, should typically be observed when the discrete-ordinates method and ENDF/B-VI libraries are used for the HBR-2 benchmark analysis.

CONTENTS

FIGURES

TABLES

ACKNOWLEDGMENTS

1 BENCHMARK DEFINITION

1.1 INTRODUCTION

This section defines the benchmark for analysis of a power reactor pressure vessel surveillance dosimetry based on data from the H. B. Robinson Unit 2 (HBR-2) power plant. This benchmark will be referred to as the HBR-2 benchmark. Analysis of the HBR-2 benchmark can be used as partial fulfillment of the requirements for the qualification of the methodology for calculating neutron fluence in pressure vessels, as required by the U.S. Nuclear Regulatory Commission Regulatory Guide DG-1053.[*]

The scope of the HBR-2 benchmark is to validate the capabilities of the calculational methodology to predict the specific activities of the radiometric dosimeters irradiated in a surveillance capsule location (in-vessel) and in a cavity location (ex-vessel), starting from the data that are typically available for an analysis of a power reactor pressure vessel surveillance dosimetry.

The input data provided consist of reactor geometry, material composition, core power distribution, and power history for the time of irradiation. The data given in Section 1 of this document and on the floppy disk accompanying this report are sufficient for the HBR-2 benchmark analysis.[†] References to other documents are provided but are not necessary for the benchmark calculation.

Experimental data provided are the measured (M) specific activities of the radiometric monitors at the end of irradiation. The dosimeters were irradiated during cycle 9 on the midplane of the HBR-2 core in the surveillance capsule and in the cavity location.

The principal results required from the benchmark analysis are the calculated (C) specific activities at the end of the cycle and the C/M ratios, for all the measurements provided. The reaction rates as obtained from the transport calculations should also be given. Short descriptions of the method and model used should accompany the numerical results.

The cross-section sets, modeling techniques, and approximations to be used in the HBR-2 benchmark analysis will be selected by the analyst; however, they are essential components of the qualified methodology and must be used in a consistent way.

---

[*]U.S. Nuclear Regulatory Commission, *Calculational and Dosimetry Methods for Determining Pressure Vessel Neutron Fluence*, Draft Regulatory Guide DG-1053, to be published.

[†]The description of the core power distribution requires a large amount of data, which are provided on the floppy disk.

1.2 DESCRIPTION

HBR-2 is a 2300-MW (thermal) pressurized light-water reactor (PWR) designed by Westinghouse and placed in operation in March of 1971. It is owned by Carolina Power and Light Company. The data presented in this section were obtained from Refs. 1 and 2, and from personal communications.[‡][**]

The core of the HBR-2 reactor consists of 157 fuel elements and is surrounded by the core baffle, core barrel, thermal shield, pressure vessel, and biological shield. Selected general data and dimensions of the HBR-2 reactor are given in Table 1.1. An octant of the horizontal cross-section of the reactor is shown schematically in Fig. 1.1, which also shows the locations of the capsule and cavity dosimeters. Axial geometry and dimensions are given in Fig. 1.2. The core baffle geometry is further specified in Fig. 1.3. Surveillance capsules are located in the downcomer region and are attached to the thermal shield. The details of the capsule mounting are shown in Fig. 1.4.

The reactor cavity is 17.10 cm (6.73 in.) wide, measured from the pressure vessel outer radius to the inner radius of the cylindrical biological (concrete) shield. A 7.62-cm (3-in.) thick insulation is installed in the cavity, leaving a 1.31-cm (0.52-in.) air gap between the pressure vessel and the insulation and an 8.18-cm (3.22-in.) air gap between the insulation and the concrete shield. The insulation consists of three steel sheets and eight steel foils with air gaps between them. The total thickness of the insulation steel sheets and foils is 0.2286 cm (0.090 in.). There are two relatively wide (38 cm, or 15 in.) and deep (80.645 cm, or 2 ft, 7.75 in.) detector wells at 0° and 45° azimuthal locations. In each well is a vertical cylinder with a 19.05-cm (7.5-in.) outer diameter and 0.635-cm (0.25-in.)-thick steel wall. The vertical axis of the cylinder is at 252.174 cm (8 ft, 3.28125 in.) from the core center. The concrete surfaces of the detector well are covered with a 0.635-cm (0.25-in.)-thick steel liner. Other concrete surfaces are bare.

The material composition of the reactor components (e.g., pressure vessel, thermal shield, etc.) is given in Table 1.2. Some components (e.g., fuel elements), have an elaborate design, but they are usually approximated as homogenized regions in the transport calculations of the out-of-the-core neutron field. To reduce the amount of data needed for such regions, the volume fractions of the materials are given in Table 1.2. The regions given in Table 1.2 correspond to the ones shown in Figs. 1.1 and 1.2. The core-average water temperature during cycle 9 was ~ 280°C (536°F), and the temperature of the water in the downcomer was approximately 267°C (512°F).[‡] The pressure was 15.513 MPa (2250 psia). The cycle average boron concentration in the coolant was approximately 500 ppm. The corresponding water densities in different regions are also given in Table 1.2. The

---

[‡]S. L. Anderson, Westinghouse Electric Corporation, personal communication to I. Remec, Oak Ridge National Laboratory, 1996.

[**]R. M. Kirch, H. B. Robinson Steam Electric Plant, Unit No. 2, response to request for information regarding operating cycle 9, personal communication to J. V. Pace, Oak Ridge National Laboratory, Oct. 1, 1996.

densities and chemical compositions of the other materials are given in Table 1.3. The concrete of the biological shielding is assumed to be type 02-B ordinary concrete (Ref. 3) with water content reduced to 4.67% by weight and iron concentration increased to reflect an estimated 0.7% by volume addition of rebar (Ref. 1).

1.3 CORE POWER DISTRIBUTION AND POWER HISTORY

The fuel assemblies in the core are numbered as shown in Fig. 1.5. These numbers are used in the description of the core power distribution during cycle 9. The data files referred to in the following discussion are provided as ASCII files on the floppy disk.

For each assembly in the core, the mass of uranium, burnup at the beginning of cycle life (BOL) and end of cycle life (EOL), burnup increment in cycle 9, and cycle-average relative power are listed in the data file FILE1.DAT. Part of the file is shown in Fig. 1.6. These data were taken from the TOTE output, except for the cycle-average assembly power. It was calculated from the BOL and EOL assembly-average burnup, taking into account the assembly uranium content. Assembly powers are normalized to the core-wise average of 1.00.

Cycle-average, assembly-wise axial power distributions are given in FILE2.DAT. Part of FILE2.DAT is shown in Fig 1.7. Each assembly is divided vertically into 12 equal-length segments, covering the active length of the fuel, with the first segment on the top and the twelfth segment at the bottom. Cycle-average relative power for each segment is given. Assembly segment powers are normalized to the average value 1.00. Relative powers of the segments were calculated from the relative cumulative axial burnup distributions given in the TOTE output for each assembly.

The cycle-average assembly-pin-power distributions are given in FILE3.DAT. The content of the file is illustrated in Fig. 1.8. Distributions are given for the assemblies in the top right quadrant of the core (e.g., assemblies 2, 3, 7, 8, 9, 10, ... ,79, 80, 81, 82, 83, 84, 85, 86) only. For each assembly, an array of 15 × 15 relative pin powers is given. Pin powers are normalized so that the average of the fuel-pin powers (e.g., 204 per assembly) is 1.00. The pin powers are ordered in rows: the first value corresponds to the pin in the top left corner of the assembly, the last value in row 1 to the pin at the top right corner of the assembly, and the last value in row 15 to the pin at the bottom right corner of the assembly. The orientation of the assembly in the core is as shown in Fig. 1.5. The cycle-average pin powers were obtained by weighting the pin powers which were given at eight core burnup steps during the cycle. The weight assigned to the power distribution at the I-th burnup step was proportional to the burnup increment from the midpoint of the ($I-1$)-th and I-th burnup step and I-th and ($I+1$)-th burnup step.

For cycle 9, a low-leakage core loading pattern was used in which 12 previously burned fuel elements (i.e., elements number 1, 2, 3, 57, 71, 72, 86, 87, 101, 155, 156, and 157) were put on the core periphery. During cycle 9, the relative powers of the outer assemblies changed significantly. This effect, which is often referred to as power redistribution, is caused by the fuel burnout and gradual changes of the boron concentration in the coolant during the cycle. The power redistribution affects

the core neutron leakage and consequently the dosimeter reaction rates. For this reason, the cycle-average core power distribution data, described previously, are supplemented by the power distribution data at several burnup steps during the cycle. At the core-average cycle burnups of 147, 417, 1632, 3363, 5257, 7595, 9293, and 10379 megawatt days per metric ton of uranium (MWd/MTU) the following information is provided: average assembly powers (FILE4.DAT, see Fig. 1.9), assembly burnups (FILE5.DAT, see Fig. 1.10), pin-power distributions for the assemblies in the upper left quadrant of the core (FILE6.DAT, see Fig. 1.11), and assembly-wise axial power distributions in 12 axial segments (FILE7.DAT, see Fig. 1.12).

The core power history for cycle 9 is given in the FILE8.DAT as is illustrated in Fig. 1.13.

Descriptions of the contents and formats of the files are given at the end of each file and are shown in Figs. 1.6–1.13.

1.4 DOSIMETRY

During cycle 9, comprehensive sets of dosimeters were irradiated in the surveillance capsule position and in several locations in the reactor cavity (Ref. 2). For the benchmark, a subset of the measurements was chosen. The selected subset consists of the threshold radiometric monitors from the surveillance capsule at the azimuthal angle of 20° and from the cavity dosimetry located at the azimuthal angle of 0°.

A specially built surveillance capsule containing no metallurgical specimens, but otherwise identical to a standard Westinghouse capsule, was placed in a previously used holder at the 20° azimuthal angle location in the downcomer. The region that usually contains metallurgical specimens was filled with carbon steel, and the dosimeters were installed in the holes drilled in the steel. Specific activities given in Table 1.4 are for the core-midplane set.[tt] Radially, the dosimeters were installed at the capsule centerline at the radius of 191.15 cm (see Fig. 1.4). The specially built capsule was irradiated during cycle 9 only.

[tt]Dosimetry sets were installed in the capsule at the core midplane and approximately 28 cm (11 in.) above and below the midplane. The measured activities showed axial variations of only ~ 3%, which is not considered important, and therefore only the results for the midplane set are given.

Specific activities of the cavity dosimeters irradiated at 0° azimuth, on the core midplane,[‡‡] are also given in Table 1.4. The dosimeters were irradiated in an aluminum 6061 holder 5.08 cm (2 in.) wide, 1.422 cm (0.56 in.) thick, and 15.240 cm (6 in.) long. Aluminum was selected as the holder material in order to minimize neutron flux perturbations at the dosimeter locations. The holder was supported by a 0.813-mm (0.032-in.)-diam. stainless steel gradient wire mounted vertically in the gap between the insulation and the biological shield at a radius of 238.02 cm (93.71 in.). The sketch of the 0° azimuth cavity dosimetry axial locations is given in Fig. 1.14.

Specific activities listed in Table 1.4 are as-measured with no corrections (e.g., for impurities or photofission). The corrections, which were estimated and used in a previous analysis (Ref. 1) are given in the footnotes to Table 1.4; however, their use is left to the analyst. The specific activities are given for the end of HBR-2 cycle 9 (January 26, 1984, at 12 P.M.).

1.5 REFERENCES

1. R. E. Maerker, "LEPRICON Analysis of the Pressure Vessel Surveillance Dosimetry Inserted into H. B. Robinson-2 During Cycle 9," *Nuc. Sci. Eng.*, 96:263 (1987).

2. E. P. Lippincott et al., *Evaluation of Surveillance Capsule and Reactor Cavity Dosimetry from H. B. Robinson Unit 2, Cycle 9*, NUREG/CR-4576 (WCAP-11104), Westinghouse Corp., Pittsburgh, Pa., February 1987.

3. *Reactor Physics Constants*, 2nd ed., ANL-5800, p.600, Argonne National Laboratory, 1963.

[‡‡]In the present benchmark, only the midplane measurements are considered. However, at the 0° azimuth multiple dosimeter sets were irradiated at the midplane and at 213 cm (7 ft) and 107 cm (3.5 ft) above and below the midplane; and activities of the gradient wire [^{54}Fe$(n,p)^{54}$Mn and ^{58}Ni$(n,p)^{58}$Co reactions] were measured at several positions between the foil locations. Adding these measurements to the benchmark would enlarge the scope of the benchmark to include verification of the calculational methodology for off-midplane locations.

Table 1.1   Selected general data and dimensions of the H. B. Robinson Unit 2

Plant		
Location	South Carolina, Hartsville	
Owner	Carolina Power and Light	
Beginning of operation	March 1971	
Reactor		
Vendor	Westinghouse	
Type	PWR	
Coolant	H_2O	
Number of loops	3	
Thermal power	2300 MW	
Core		
Number of fuel assemblies	157	
Pitch	21.504 cm	8.466 in.
Fuel Element		
Type	15 × 15 array of fuel pins	
Fuel pins per element	204	
Horizontal cross section (including gap)	rectangular, 21.504 cm × 21.504 cm	
Height of fuel	365.76 cm	12 ft.
Core Baffle*		
Dimensions	See Fig. 1.3	
Thickness	2.858 ± 0.013 cm	1.125 ± 0.005 in.
Core Barrel†		
Inner radius	170.023 ± 0.318 cm	66.938 ± 0.125 in.
Thickness	5.161 ± 0.107 cm	2.032 ± 0.042 in.
Thermal Shield		
Inner radius	181.135 ± 0.318 cm	71.313 ± 0.125 in.
Thickness	6.825 ± 0.160 cm	2.687 ± 0.063 in.
Pressure Vessel		
Cladding		
Inner radius	197.485 ± 0.076 cm	77.750 ± 0.030 in.
Thickness (minimal)	0.556 cm	7/32 in. (0.219 in.)
Base metal		
Inner radius‡	198.041 cm	77.969 in.
Thickness**	23.614 ± 0.041 cm	9.297 ± 0.016 in.
Total thickness (wall + cladding)	24.170 cm	9.516 in.

Table 1. 1 (continued)

Pressure Vessel Thermal Insulation		
Inner radius	222.964 cm	87.781 in.
Total insulation thickness (including voids)	7.620 cm	3.0 in.
Insulation steel components		
1 steel sheet	0.079 cm	0.031 in.
1 steel sheet	0.046 cm	0.018 in.
1 steel sheet	0.064 cm	0.025 in.
8 steel foils	0.005 cm	0.002 in.
Total thickness of the steel in the insulation	0.229 cm	0.090 in.
Pressure Vessel Cavity Dimensions	See Fig. 1.1	
Vessel-to-insulation gap	1.31 cm	0.52 in.
Insulation	7.62 cm	3.00 in.
Insulation-to-concrete gap	8.18 cm	3.22 in.
Total width of the cylindrical part	17.10 cm	6.73 in.
Biological Shield Dimensions	See Fig. 1.1	
Inner radius of cylindrical surfaces	238.760 cm	7 ft 10 in.

* The baffle units are positioned symmetrically about the core center within 0.025 cm (0.010 in.) measured at the top and bottom former elevations.

† The annular gap between the core barrel outer radius and the thermal shield inner radius is maintained uniform within 0.381 cm (0.150 in.).

‡ The pressure vessel base metal inner radius is obtained as the cladding inner radius plus specified minimum cladding thickness of 0.556 cm (7/32 in.).

** The pressure vessel thickness is based on a single measurement of the lower shell and three measurements of the intermediate shell (S. L. Anderson, Westinghouse Electric Corporation, personal communication to I. Remec, Oak Ridge National Laboratory, 1996).

Table 1.2 Materials of the components and regions

Region	Material*	Volume fraction
Reactor core	UO_2, enriched to 2.9%, density 10.418 g cm^{-3}	0.2997
	Zircaloy-4	0.1004
	Inconel-718	0.00281
	Stainless steel SS-304	0.00062
	Water density 0.766 g cm^{-3}	0.5886
Core baffle	Stainless steel SS-304	1.00
Bypass region	Water density 0.776 g cm^{-3}	See Fig. 1.2
Core barrel	Stainless steel SS-304	1.00
Downcomer region No. 1	Water density 0.787 g cm^{-3}	1.00
Thermal shield	Stainless steel SS-304	1.00
Surveillance capsule Mounting Content	Stainless steel SS-304 Steel A533B	1.00 1.00
Downcomer region No. 2	Water density 0.787 g cm^{-3}	1.00
Pressure vessel cladding	Stainless Steel SS-304	1.00
Pressure vessel	Steel A533B	1.00
Insulation	Stainless steel SS-304 Air	0.03 0.97
Reactor cavity	Air	1.00
Biological shield	Concrete	1.00

Table 1.2 (continued)

Region	Material	Volume Fraction
Core support	Stainless steel SS-304 Water density 0.787 g cm^{-3}	0.049 0.951
Lower core plate	Stainless steel SS-304 Water density 0.787 g cm^{-3}	0.668 0.332
Nozzle legs	Stainless steel SS-304 Water density 0.787 g cm^{-3}	0.070 0.930
Bottom nozzle plate	Stainless steel SS-304 Water density 0.787 g cm^{-3}	0.717 0.283
Water gap No. 1	Stainless steel SS-304 Water density 0.787 g cm^{-3}	0.007 0.993
End plugs	Stainless steel SS-304 Water density 0.787 g cm^{-3}	0.300 0.700
Fuel plenum	Stainless steel SS-304 Water density 0.745 g cm^{-3}	0.224 0.560
Water gap No.2	Stainless steel SS-304 Water density 0.745 g cm^{-3}	0.017 0.983
Top nozzle	Stainless steel SS-304 Water density 0.745 g cm^{-3}	0.275 0.725
Formers	Stainless steel SS-304 Water density 0.766 g cm^{-3}	0.900 0.100

* The boron concentration in the coolant was approximately 500 ppm (cycle average).

Table 1.3 Densities (gcm^{-3}) and chemical compositions (wt %) of reactor component materials

	Carbon steel A533B	Stainless steel SS-304	Inconel-718	Zircaloy-4	Concrete*
Density	7.83	8.03	8.3	6.56	2.275
Element					
Fe	97.90	69.0	7.0	0.50	3.82
Ni	0.55	10.0	73.0		
Cr		19.0	15.0		
Mn	1.30	2.0			
C	0.25				0.10
Ti			2.5		
Si			2.5		34.09
Zr				97.91	
Sn				1.59	
Ca					4.40
K					1.31
Al					3.43
Mg					0.22
Na					1.62
O					50.50
H					0.51

* The concrete is assumed to be type 02-B ordinary concrete (Ref. 3) with water content reduced to 4.67% by weight and iron concentration increased to reflect an estimate 0.7% by volume addition of rebar (Ref. 1).

Table 1.4 Measured specific activities of the dosimeters from the surveillance capsule and from the cavity, at the end of cycle 9 (1/26/1984). Specific activities (Bq/mg) are given per mg of Ni, Fe, Ti, and Cu material with naturally occurring isotopic composition, and per mg of ^{237}Np and ^{238}U isotopes.

Dosimeter	Surveillance capsule (core midplane, 20° azimuth, radius 191.15 cm)[*]	Cavity (core midplane, 0° azimuth, radius 238.02 cm)[†]
^{237}Np(n,f) ^{137}Cs	3.671×10^2	2.236×10^1
^{238}U(n,f) ^{137}Cs	5.345×10^1	8.513×10^{-1}
^{58}Ni (n,p) ^{58}Co	1.786×10^{4}[‡]	1.959×10^2
^{54}Fe (n,p) ^{54}Mn	9.342×10^{2}[‡]	8.711
^{46}Ti (n,p) ^{46}Sc	3.500×10^{2}[**]	3.310
^{63}Cu (n,α) ^{60}Co	2.646×10^{1}[**]	2.645×10^{-1}

[*] Dosimeters in the capsule were irradiated under 0.508 mm (0.020 in.) Gd cover, except where noted differently. Ref. 1 estimates that in order to compensate for the photofission contribution, the ^{137}Cs activity in ^{237}Np and ^{238}U should be reduced by 2.5% and 5%, respectively; and ^{60}Co activity in ^{63}Cu should be reduced by 2.5% to compensate for the contribution from the ^{59}Co$(n,\gamma)^{60}$Co reaction on the Co impurities in the Cu dosimeter.

[†] In the cavity, the ^{237}Np, ^{238}U, and Ni dosimeters were irradiated under 0.508 mm (0.020 in.) Cd cover. Ti and Fe dosimeters were irradiated bare. Activity of the Fe is an average of four measurements. The Cu activity is an average of one bare dosimeter and one dosimeter irradiated in Cd cover. Ref. 1 estimates that in order to compensate for the photofission contribution, the ^{137}Cs activity in ^{237}Np and ^{238}U should be reduced by 5.0% and 10.0%, respectively; and ^{60}Co activity in ^{63}Cu should be reduced by 2.5% to compensate for the contribution from the ^{59}Co$(n,\gamma)^{60}$Co reaction on the Co impurities in the Cu dosimeter.

[‡] Average of five dosimeters, three inside Gd and two outside.

[**] Average of two measurements.

Regions:
1 . . . . reactor core
2 . . . . core baffle
3 . . . . bypass region
4 . . . . core barrel
5 . . . . downcomer reg. #1
6 . . . . thermal shield
7 . . . . downcomer reg. #2
8 . . . . pressure vessel
9,11 . . . cavity (air)
10 . . . . vessel insulation
12 . . . . biological shield
13 . . . . steel-wall cylinder
14 . . . . detector well
x . . . . . capsule and cavity
        dosimeters locations
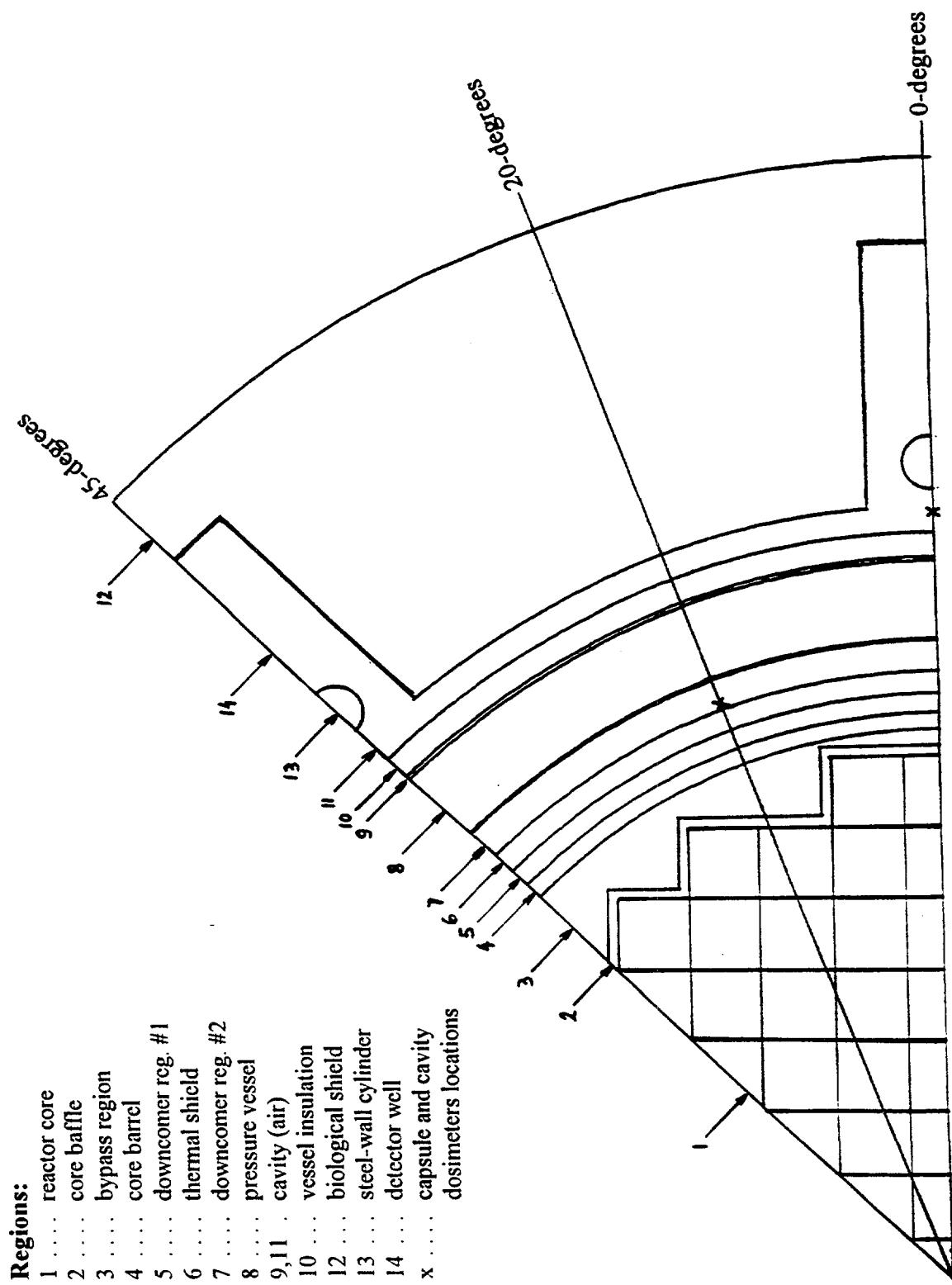
Fig. 1.1 **Horizontal cross section of the HBR-2 reactor.** One octant of the core is shown

0-degrees

20-degrees

45-degrees
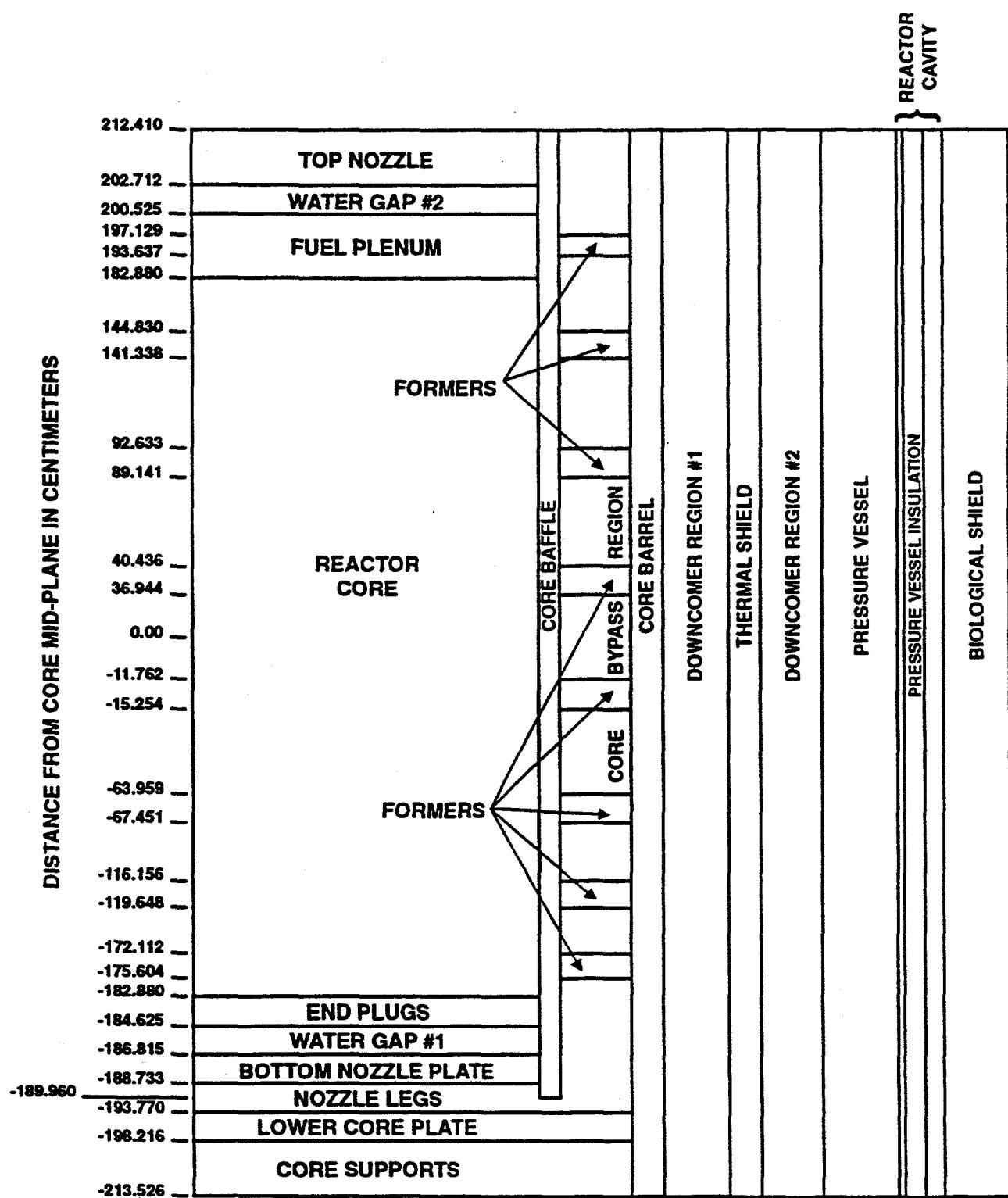
Fig. 1.2   Schematic sketch of the axial geometry (not to scale). Dimensions are in centimeters
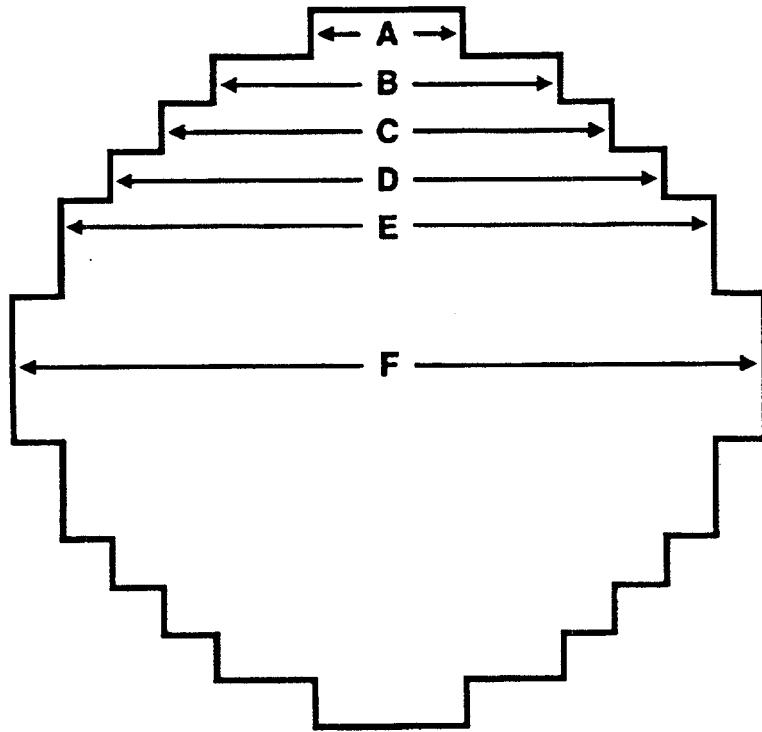
DIMENSION

A	64.607 ± 0.036 cm	(25.436 ± 0.014 in.)
B	150.663 ± 0.046 cm	(59.316 ± 0.018 in.)
C	193.680 ± 0.056 cm	(76.252 ± 0.022 in.)
D	236.698 ± 0.066 cm	(93.188 ± 0.026 in.)
E	279.715 ± 0.076 cm	(110.124 ± 0.030 in.)
F	322.684 ± 0.084 cm	(127.041 ± 0.033 in.)

Fig. 1.3   Core baffle geometry. Nominal dimensions are given for the core-side surfaces of the baffle plates. Deviations from nominal are for the maximum and minimum dimensions (e.g., for A the nominal dimension is 64.607 cm, with the maximum value of 64.643 cm and the minimum value of 64.571 cm)
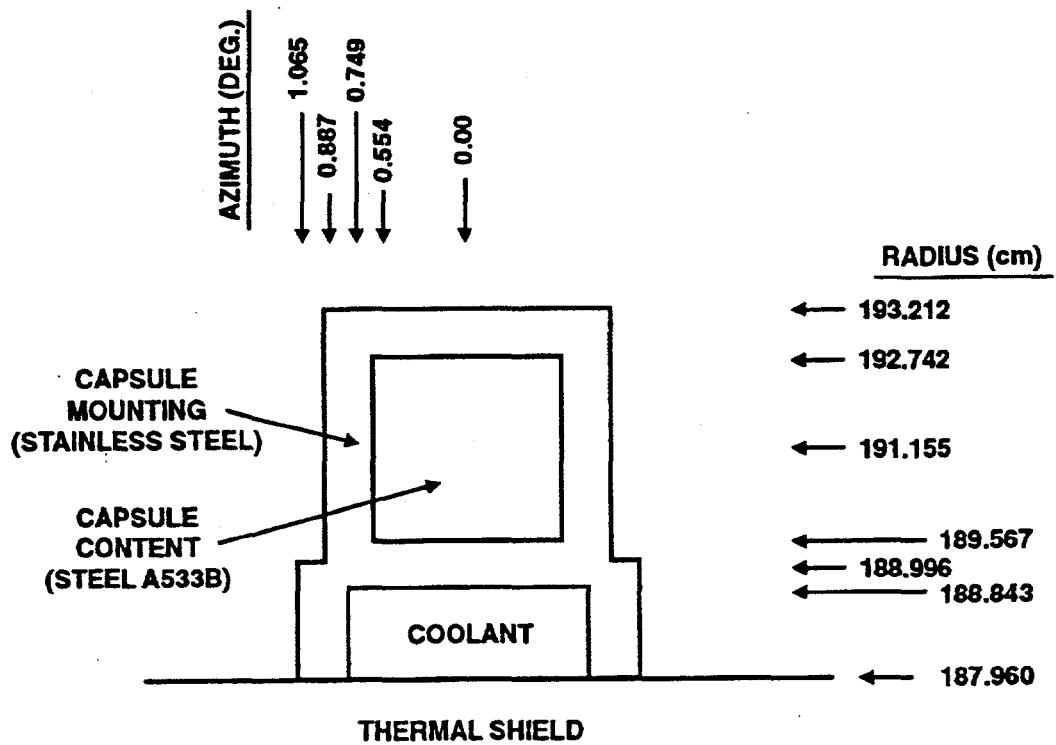
Fig. 1.4 Sketch of the surveillance capsule mounting on the thermal shield (not to scale). The capsule centerline is at 191.155 ± 0.152 cm (75.258 ± 0.060 in.) (S. L. Anderson, Westinghouse Electric Corporation, personal communication to I. Remec, Oak Ridge National Laboratory, 1996)

NUREG/CR-6453

						1	2	3						
				4	5	6	7	8	9	10				
			11	12	13	14	15	16	17	18	19			
		20	21	22	23	24	25	26	27	28	29	30		
	31	32	33	34	35	36	37	38	39	40	41	42	43	
	44	45	46	47	48	49	50	51	52	53	54	55	56	
57	58	59	60	61	62	63	64	65	66	67	68	69	70	71
72	73	74	75	76	77	78	79	80	81	82	83	84	85	86
87	88	89	90	91	92	93	94	95	96	97	98	99	100	101
	102	103	104	105	106	107	108	109	110	111	112	113	114	
	115	116	117	118	119	120	121	122	123	124	125	126	127	
		128	129	130	131	132	133	134	135	136	137	138		
			139	140	141	142	143	144	145	146	147			
				148	149	150	151	152	153	154				
						155	156	157						

Fig. 1.5 The numbering of the fuel elements in the HBR-2 core

```
ASS. #       MTU      BU-BOL    BU-EOL      dBU      Ave. P
     1     0.4285    29488.    33102.     3614.     0.337
     2     0.4269    22091.    26798.     4707.     0.438
     3     0.4288    29122.    32688.     3566.     0.333
                                    .
                                    .
                                    .

   155     0.4285    29057.    32748.     3691.     0.345
   156     0.4281    22727.    27443.     4716.     0.440
   157     0.4291    29270.    32842.     3572.     0.334
EOF
```

Legend:
ASS. #.....assembly number as in Fig. 1.5.
MTU........mass of uranium in the assembly
           in metric tonnes.
BU-BOL.....assembly burnup in MWd/MTU at the beginning
           of cycle (BOL).
BU-EOL.....assembly burnup in MWd/MTU at the end of
           cycle (EOL).
dBU........assembly burnup increase in cycle 9 in
           MWd/MTU.
Ave. P.....cycle-average assembly power.

Format: (I6,F9.4,3F9.0,F9.3)

Fig. 1.6 Content and format of the FILE1.DAT. Beginning and end of file are shown

```
ASS. #  Cycle-average, assembly axial-segment-powers

  1 0.696895 0.995964 1.064975 1.054674 1.076852 1.063509
    1.087683 1.073097 1.090714 1.071349 1.012495 0.711793
  2 0.690069 0.992619 1.064409 1.053981 1.080842 1.062351
    1.092513 1.074481 1.088941 1.070761 1.012128 0.716907
  3 0.597160 0.942708 1.056288 1.058032 1.084421 1.075771
    1.101560 1.090651 1.100337 1.093457 1.032470 0.767144

                              .
                              .
                              .

155 0.766128 1.028479 1.076598 1.088410 1.084673 1.077273
    1.102337 1.077251 1.093745 1.056529 0.955013 0.593564
156 0.695985 0.991515 1.066876 1.080861 1.088512 1.080346
    1.104275 1.084720 1.098602 1.071259 0.984913 0.652136
157 0.572353 0.931786 1.054233 1.069350 1.094944 1.084444
    1.106110 1.094919 1.103209 1.094470 1.029888 0.764293
EOF
```

Legend:
Ass. # ....assembly number as in Fig. 1.5.

Cycle-average, assembly axial-segment powers (12 segments per assembly) are relative powers of axial segments of the assembly. Each segment is 30.48 cm long (1 ft). First segment (after Ass. #) is at the top of active fuel and last segment is at the bottom of the fuel. Normalization is to the average segment power of 1.00 in every assembly (e.g., the sum of segment powers in any assembly is 12).

Format: (I3,6F9.6/3X,6F9.6)

Fig. 1.7 Content and format of the FILE2.DAT. Beginning and end of file are shown

```
CYCLE-AVERAGE PIN POWERS

ASSEMBLY NUMBER    2
 1  .2896  .2963  .3044  .3108  .3162  .3202  .3219  .3224  .3223  .3211  .3173  .3124  .3062  .2985  .2920
 2  .4325  .4446  .4608  .4628  .4693  .4798  .4758  .4721  .4764  .4810  .4710  .4650  .4636  .4476  .4359
 3  .5393  .5615  .0000  .5859  .5935  .0000  .6055  .6004  .6061  .0000  .5956  .5888  .0000  .5654  .5433
 4  .6267  .6441  .6698  .6797  .6957  .7006  .7009  .0000  .7017  .7022  .6981  .6830  .6739  .6487  .6312
 5  .7077  .7274  .7561  .7754  .0000  .7768  .7671  .7743  .7680  .7785  .0000  .7791  .7607  .7326  .7128
 6  .7884  .8198  .0000  .8609  .8563  .8428  .8338  .8348  .8347  .8447  .8593  .8650  .0000  .8254  .7938
 7  .8676  .8910  .9323  .9441  .9267  .9137  .9222  .9346  .9231  .9157  .9299  .9485  .9377  .8970  .8735
 8  .9488  .9653 1.0090  .0000 1.0204  .9976 1.0191  .0000 1.0201  .9997 1.0237  .0000 1.0148  .9715  .9549
 9 1.0329 1.0596 1.1076 1.1206 1.0993 1.0834 1.0931 1.1074 1.0941 1.0854 1.1027 1.1255 1.1136 1.0661 1.0391
10 1.1185 1.1604  .0000 1.2142 1.2061 1.1859 1.1726 1.1736 1.1737 1.1881 1.2096 1.2192  .0000 1.1671 1.1248
11 1.2009 1.2303 1.2749 1.3039  .0000 1.3016 1.2842 1.2957 1.2853 1.3038  .0000 1.3090 1.2811 1.2371 1.2071
12 1.2853 1.3149 1.3614 1.3765 1.4047 1.4118 1.4107  .0000 1.4118 1.4141 1.4084 1.3815 1.3677 1.3217 1.2914
13 1.3729 1.4201  .0000 1.4660 1.4790  .0000 1.5020 1.4883 1.5030  .0000 1.4826 1.4710  .0000 1.4269 1.3788
14 1.4609 1.4875 1.5288 1.5242 1.5369 1.5649 1.5480 1.5343 1.5490 1.5670 1.5403 1.5291 1.5349 1.4940 1.4665
15 1.5606 1.5704 1.5888 1.6018 1.6130 1.6223 1.6233 1.6233 1.6243 1.6244 1.6163 1.6066 1.5947 1.5768 1.5660



ASSEMBLY NUMBER   86
 1 1.5463 1.4474 1.3604 1.2750 1.1928 1.1120 1.0279  .9449  .8658  .7881  .7084  .6279  .5406  .4339  .2907
 2 1.5542 1.4724 1.4083 1.3042 1.2227 1.1558 1.0563  .9635  .8913  .8222  .7303  .6474  .5657  .4480  .2992
 3 1.5704 1.5138  .0000 1.3520 1.2692  .0000 1.1057 1.0100  .9345  .0000  .7618  .6756  .0000  .4664  .3085
 4 1.5820 1.5068 1.4531 1.3662 1.2985 1.2108 1.1206  .0000  .9483  .8663  .7825  .6866  .5934  .4691  .3158
 5 1.5916 1.5188 1.4666 1.3960  .0000 1.2029 1.0982 1.0222  .9305  .8626  .0000  .7050  .6028  .4770  .3221
 6 1.5989 1.5467  .0000 1.4018 1.2953 1.1818 1.0825  .9997  .9180  .8491  .7857  .7109  .0000  .4893  .3271
 7 1.5978 1.5275 1.4868 1.4016 1.2773 1.1692 1.0930 1.0223  .9277  .8414  .7768  .7131  .6172  .4861  .3296
 8 1.5953 1.5125 1.4736  .0000 1.2895 1.1709 1.1086  .0000  .9415  .8438  .7858  .0000  .6139  .4835  .3309
 9 1.5957 1.5267 1.4870 1.4027 1.2792 1.1716 1.0959 1.0256  .9312  .8452  .7806  .7172  .6210  .4895  .3321
10 1.5948 1.5450  .0000 1.4041 1.2991 1.1867 1.0883 1.0062  .9251  .8565  .7935  .7187  .0000  .4959  .3320
11 1.5857 1.5164 1.4673 1.3995  .0000 1.2104 1.1071 1.0322  .9411  .8739  .0000  .7165  .6137  .4866  .3292
12 1.5742 1.5036 1.4541 1.3708 1.3062 1.2210 1.1327  .0000  .9629  .8813  .7978  .7015  .6076  .4814  .3248
13 1.5608 1.5098  .0000 1.3577 1.2787  .0000 1.1206 1.0264  .9522  .0000  .7802  .6938  .0000  .4815  .3193
14 1.5424 1.4674 1.4095 1.3106 1.2334 1.1703 1.0732  .9822  .9116  .8435  .7517  .6684  .5861  .4658  .3121
15 1.5313 1.4407 1.3609 1.2815 1.2045 1.1278 1.0469  .9663  .8888  .8122  .7331  .6525  .5643  .4551  .3065
EOF
```

Legend:
For each assembly in the top right quadrant of the core an array of 15 x 15 relative pin powers p(i,j) is given. The assembly is oriented as in Fig. 1.5, pin(1,1) is in the top left corner, pin(1,15) in the top right corner, pin(15,1) in the bottom left corner and pin(15,15) in the bottom right corner.

For each assembly in the top right quadrant of the core the following is given:

ASSEMBLY NUMBER   #..........assembly number as in Fig. 1.5; one record.
Format: (' ASSEMBLY NUMBER ',I3)

Row number i, pin powers p(i,j),j=1,15; fifteen records.
Format: (I3,15F7.4).

Fig. 1.8 Content and format of the FILE3.DAT. Beginning and end of file are shown

```
ASSEMBLY RELATIVE POWERS FOR BURNUP STEP    1 (   147 MWd/MTU)

CORE AVERAGE ASSEMBLY POWER   1.000


                                  .241  .329  .244
                      .705  .874  .853  .910  .855  .876  .707
                .784 1.180 1.289 1.014  .883 1.016 1.292 1.183  .786
          .781 1.054 1.190 1.116 1.266  .995 1.269 1.118 1.193 1.058  .784
     .701 1.173 1.181 1.038 1.201 1.028 1.138 1.031 1.207 1.052 1.190 1.177  .703
     .868 1.280 1.108 1.196 1.113 1.258 1.086 1.264 1.120 1.207 1.114 1.283  .867
.239 .846 1.008 1.260 1.024 1.257 1.171 1.371 1.177 1.263 1.029 1.263 1.007  .842 .235
.317 .897  .876  .991 1.134 1.082 1.365 1.133 1.374 1.086 1.136  .992  .876  .896 .317
.239 .844 1.006 1.261 1.027 1.259 1.171 1.367 1.174 1.262 1.027 1.261 1.008  .845 .239
     .868 1.280 1.112 1.203 1.114 1.256 1.082 1.258 1.115 1.198 1.108 1.280  .867
     .702 1.175 1.187 1.047 1.198 1.024 1.131 1.024 1.198 1.036 1.179 1.172  .701
          .783 1.055 1.187 1.110 1.257  .984 1.256 1.109 1.183 1.050  .780
                .783 1.177 1.282 1.003  .857 1.002 1.279 1.173  .780
                      .703  .868  .845  .896  .843  .867  .701
                                  .241  .322  .241
                                        .
                                        .
                                        .

ASSEMBLY RELATIVE POWERS FOR BURNUP STEP    8 (10379 MWd/MTU)

CORE AVERAGE ASSEMBLY POWER   1.000


                                  .382  .508  .386
                      .741 1.016 1.184 1.234 1.185 1.016  .741
                .847 1.121 1.215 1.050  .971 1.051 1.215 1.120  .847
          .847 1.262 1.135 1.018 1.159  .961 1.158 1.017 1.134 1.262  .847
     .741 1.121 1.132  .969 1.060  .957 1.257  .957 1.060  .975 1.133 1.120  .741
    1.017 1.215 1.016 1.059  .963 1.072  .958 1.073  .964 1.061 1.017 1.214 1.016
.387 1.188 1.053 1.159  .957 1.072  .950 1.070  .951 1.072  .957 1.159 1.051 1.184 .382
.514 1.237  .972  .962 1.257  .958 1.068  .869 1.071  .958 1.257  .962  .972 1.237 .514
.386 1.186 1.051 1.159  .957 1.073  .950 1.069  .951 1.074  .957 1.160 1.053 1.188 .387
    1.017 1.214 1.018 1.062  .965 1.072  .959 1.074  .965 1.060 1.017 1.215 1.018
     .741 1.121 1.134  .975 1.060  .957 1.258  .958 1.061  .970 1.132 1.121  .742
          .847 1.263 1.135 1.018 1.159  .959 1.159 1.019 1.135 1.263  .848
                .848 1.122 1.216 1.050  .956 1.049 1.216 1.122  .848
                      .742 1.017 1.185 1.233 1.185 1.018  .742
                                  .386  .504  .386
EOF
```

Legend:

Assembly relative powers at eight core burnups.
Assembly relative powers are normalized to
the average core-wise value of 1.00.

Format: free format

Fig. 1.9 Content and format of the FILE4.DAT. Beginning and end of file are shown

```
CYCLE   9 AT    147.00 MWd/T (MICROBURN-P  CASE  9    RNP Cycle 09 MAP413, 0773 ppm, 1761 MW, 00147 MWd/MTU)
ASSEMBLY BURNUPS IN   1000 MWd/MTU

                                  29.274 22.141 29.143
                           .106   .131   .127   .136   .128   .131   .106
                    .117  7.706  6.970 18.806 23.048 18.808  6.947  7.705   .118
              .117   .158 12.146 19.792  7.328 18.895  7.322 19.800 12.097   .158   .117
       .105  7.715 12.202 21.817 12.075 22.998   .166 22.990 12.071 21.517 12.225  7.717   .105
       .130  7.007 19.815 12.084 19.658 10.232 21.989 10.215 19.658 12.090 19.824  7.001   .130
29.272 .126 18.796  7.333 23.032 10.252 19.673  8.274 19.676 10.262 23.040  7.337 18.798   .125 29.143
21.147 .133 23.046 18.893   .166 22.074  8.373 21.264  8.329 22.080   .166 18.894 23.049   .133 21.149
29.275 .126 18.799  7.340 23.034 10.275 19.673  8.274 19.678 10.259 23.025  7.336 18.800   .126 29.275
       .130  7.040 19.835 12.085 19.655 10.216 21.989 10.230 19.653 12.081 19.835  6.999   .130
       .105  7.718 12.265 21.517 12.069 22.987   .165 22.999 12.074 21.834 12.217  7.717   .105
              .117   .158 12.103 19.786  7.321 18.898  7.325 19.803 12.138   .157   .117
                    .117  7.704  6.947 18.806 23.045 18.808  6.967  7.705   .117
                           .105   .130   .126   .133   .126   .130   .105
                                  29.143 22.775 29.145

                                          .
                                          .
                                          .

CYCLE   9 AT 10379.00 MWd/T (MICROBURN-P  CASE 34    RNP Cycle 09 MAP455, 0040 ppm, 1261 MW, 10379 MWd/MTU)
ASSEMBLY BURNUPS IN   1000 MWd/MTU

                                  32.497 26.471 32.406
                           7.376  9.749 10.704 11.323 10.727  9.757  7.380
                    8.430 19.295 19.616 29.438 32.739 29.451 19.604 19.299  8.435
              8.423 12.298 23.936 30.586 19.817 29.462 19.819 30.593 23.891 12.310  8.428
       7.369 19.285 23.945 31.964 23.464 33.192 13.041 33.199 23.475 31.745 23.999 19.291  7.364
       9.743 19.632 30.575 23.446 30.080 21.956 32.380 21.970 30.110 23.503 30.606 19.620  9.717
32.528 10.717 29.437 19.817 33.217 21.980 30.281 20.477 30.314 22.011 33.239 19.817 29.407 10.661 32.349
25.456 11.312 32.733 29.461 13.032 32.449 20.542 31.588 20.551 32.472 13.040 29.462 32.729 11.291 25.446
32.525 10.699 29.417 19.823 33.235 22.019 30.283 20.461 30.309 22.017 33.226 19.823 29.437 10.709 32.527
       9.737 19.660 30.621 23.497 30.091 21.941 32.371 21.972 30.092 23.463 30.598 19.624  9.741
       7.369 19.296 24.046 31.740 23.446 33.170 13.017 33.188 23.461 31.976 23.954 19.283  7.367
              8.431 12.313 23.888 30.560 19.775 29.412 19.777 30.575 23.905 12.284  8.418
                    8.433 19.289 19.577 29.390 32.542 29.383 19.586 19.279  8.422
                           7.371  9.731 10.666 11.240 10.659  9.725  7.366
                                  32.384 27.050 32.385
EOF
```

Legend: Assembly burnups at eight core burnup steps.

Format: free format

Fig. 1.10 **Content and format of the FILE5.DAT.** Beginning and end of file are shown

```
PIN POWERS FOR BURNUP STEP #  1 (  147 MWd/MTU)

ASSEMBLY NUMBER    2
ASSEMBLY AVERAGE FUEL-ROD POWER BEFORE NORMALIZATION   .329
 1  .2747  .2823  .2908  .2975  .3027  .3069  .3085  .3091  .3088  .3076  .3039  .2990  .2930  .2848  .2775
 2  .4115  .4249  .4416  .4437  .4501  .4607  .4568  .4534  .4574  .4622  .4519  .4461  .4446  .4282  .4151
 3  .5142  .5376  .0000  .5631  .5707  .0000  .5829  .5780  .5838  .0000  .5732  .5662  .0000  .5419  .5188
 4  .5987  .6178  .6443  .6540  .6704  .6756  .6765  .0000  .6774  .6774  .6731  .6576  .6488  .6227  .6039
 5  .6780  .6993  .7291  .7488  .0000  .7516  .7418  .7494  .7427  .7537  .0000  .7528  .7342  .7051  .6838
 6  .7585  .7920  .0000  .8351  .8315  .8178  .8099  .8111  .8111  .8199  .8348  .8394  .0000  .7984  .7646
 7  .8391  .8649  .9078  .9208  .9041  .8920  .9008  .9135  .9020  .8944  .9075  .9257  .9138  .8716  .8461
 8  .9236  .9430  .9889  .0000 1.0023  .9804 1.0026  .0000 1.0038  .9825 1.0059  .0000  .9953  .9503  .9309
 9 1.0126 1.0424 1.0928 1.1077 1.0868 1.0719 1.0819 1.0971 1.0831 1.0743 1.0907 1.1132 1.0998 1.0500 1.0199
10 1.1044 1.1506  .0000 1.2083 1.2016 1.1810 1.1688 1.1700 1.1700 1.1834 1.2059 1.2141  .0000 1.1585 1.1120
11 1.1946 1.2278 1.2761 1.3068  .0000 1.3071 1.2892 1.3013 1.2904 1.3098  .0000 1.3129 1.2834 1.2357 1.2022
12 1.2889 1.3232 1.3739 1.3898 1.4208 1.4290 1.4287  .0000 1.4299 1.4317 1.4250 1.3955 1.3815 1.3314 1.2968
13 1.3913 1.4445  .0000 1.4964 1.5110  .0000 1.5359 1.5220 1.5371  .0000 1.5153 1.5025  .0000 1.4527 1.3989
14 1.5019 1.5347 1.5806 1.5773 1.5909 1.6222 1.6040 1.5903 1.6052 1.6250 1.5952 1.5830 1.5882 1.5429 1.5095
15 1.6411 1.6554 1.6779 1.6934 1.7064 1.7168 1.7186 1.7186 1.7198 1.7195 1.7104 1.6991 1.6851 1.6636 1.6484


                             .
                             .
                             .

ASSEMBLY NUMBER   86
ASSEMBLY AVERAGE FUEL-ROD POWER BEFORE NORMALIZATION   .514
 1 1.4787 1.4069 1.3382 1.2654 1.1928 1.1195 1.0406  .9626  .8861  .8102  .7308  .6491  .5597  .4494  .3009
 2 1.4851 1.4305 1.3837 1.2938 1.2224 1.1619 1.0687  .9807  .9116  .8443  .7534  .6693  .5852  .4642  .3098
 3 1.5001 1.4692  .0000 1.3392 1.2656  .0000 1.1169 1.0264  .9542  .0000  .7839  .6975  .0000  .4829  .3196
 4 1.5104 1.4626 1.4258 1.3532 1.2940 1.2156 1.1309  .0000  .9676  .8886  .8049  .7090  .6136  .4862  .3273
 5 1.5196 1.4744 1.4375 1.3806  .0000 1.2074 1.1095 1.0383  .9503  .8847  .0000  .7271  .6230  .4945  .3342
 6 1.5264 1.4995  .0000 1.3871 1.2915 1.1874 1.0940 1.0155  .9381  .8717  .8088  .7335  .0000  .5068  .3394
 7 1.5246 1.4812 1.4573 1.3853 1.2738 1.1743 1.1037 1.0371  .9470  .8635  .7997  .7353  .6380  .5037  .3419
 8 1.5229 1.4672 1.4447  .0000 1.2855 1.1751 1.1181  .0000  .9601  .8653  .8086  .0000  .6347  .5011  .3435
 9 1.5225 1.4803 1.4573 1.3865 1.2755 1.1765 1.1064 1.0402  .9505  .8672  .8034  .7392  .6417  .5070  .3443
10 1.5221 1.4974  .0000 1.3890 1.2950 1.1920 1.0996 1.0218  .9449  .8791  .8164  .7413  .0000  .5134  .3443
11 1.5134 1.4715 1.4377 1.3835  .0000 1.2146 1.1181 1.0480  .9606  .8958  .0000  .7384  .6337  .5041  .3410
12 1.5023 1.4589 1.4262 1.3573 1.3014 1.2253 1.1426  .0000  .9817  .9032  .8199  .7238  .6276  .4982  .3363
13 1.4900 1.4643  .0000 1.3442 1.2744  .0000 1.1313 1.0424  .9715  .0000  .8020  .7156  .0000  .4980  .3303
14 1.4727 1.4246 1.3839 1.2995 1.2325 1.1759 1.0850  .9990  .9314  .8653  .7746  .6901  .6057  .4819  .3227
15 1.4630 1.3991 1.3378 1.2711 1.2037 1.1348 1.0593  .9836  .9089  .8343  .7555  .6738  .5835  .4708  .3170
EOF
```

Legend:
For eight core burnup steps the assembly pin powers are given for each
assembly in the top right quadrant of the core. For each assembly an array
of 15 x 15 relative pin powers p(i,j) is given. The assembly is oriented as
in Fig. 1.5; pin(1,1) is in the top left corner, pin(1,15) in the top right
corner, pin(15,1) in the bottom left corner and pin(15,15) in the bottom
right corner.

For each assembly in the top right quadrant of the core the following is
given:

ASSEMBLY NUMBER   #..........assembly number as in Fig. 1.5; one record.
Format: (' ASSEMBLY NUMBER ',I3)

ASSEMBLY AVERAGE FUEL-ROD POWER BEFORE NORMALIZATION.... assembly average
fuel-rod power is equal to the relative assembly power.
Format: (' ASSEMBLY AVERAGE FUEL-ROD POWER BEFORE NORMALIZATION   ',F5.3)

Row number i, pin powers p(i,j),j=1,15; fifteen records. Pin powers are
normalized so that the average of the fuel-pin powers (204 per assembly) is
1.000.
Format: (I3,15F7.4).

Fig. 1.11 Content and format of the FILE6.DAT. Beginning and end of file are shown

```
   00147MWd/MT
 1      .04662     .07495     .08855     .09196     .09584     .09618
        .09872     .09612     .09394     .08788     .07724     .05199
 2      .04607     .07432     .08827     .09209     .09602     .09636
        .09891     .09631     .09413     .08805     .07739     .05208
                                      .
                                      .
                                      .
156     .05030     .07704     .08863     .09508     .09722     .09821
        .09986     .09596     .09400     .08686     .07278     .04404
157     .03839     .06957     .08568     .09152     .09607     .09696
        .09859     .09707     .09587     .09165     .08082     .05780
                                      .
                                      .
                                      .
   10379MWd/MT
 1      .07266     .09436     .09279     .08585     .08551     .08275
        .08349     .08130     .08161     .08257     .08181     .07530
 2      .07118     .09300     .09242     .08613     .08589     .08312
        .08386     .08166     .08197     .08295     .08218     .07564
                                      .
                                      .
                                      .
157     .05238     .08230     .09055     .08942     .08940     .08700
        .08669     .08578     .08371     .08479     .08520     .08278
EOF
```

Legend:
For eight core burnup steps, the following is given.

Ass. # ....assembly number as in Fig. 1.5.
Relative powers of the axial segments of the assembly.
There are 12 segments per assembly and each segment is
30.48 cm long (1 ft). The first segment (after Ass. #) is
at the top of the active fuel and the last segment is at
the bottom of the fuel. Normalization is to the sum of the
segment powers equal to 1.00 in any assembly.

Format: (I3,6F10.5/3X,6F10.5)

Fig. 1.12 Content and format of the FILE7.DAT. Beginning and end of file are shown

```
        YYMMDD        BU       LF      DTG  Temp.
                    MWd/MTU     %      MWd  100°F
        820801        .0       .0       .0  5.250
        820802        .0       .0       .0   .000
        820803        .0       .0       .0   .000
        820804        .0       .0       .0  4.080
        820805        .0       .0       .0  5.300
        820806        .0       .0       .0  3.440


                              .
                              .
                              .


        840126  10636.8     34.0     782.2  5.354
        840127  10636.8       .0       .0  5.030
        840128  10636.8       .0       .0   .000
        840129  10636.8       .0       .0   .000
        840130  10636.8       .0       .0  1.260
        840131  10636.8       .0       .0  1.170
        EOF
```

Legend:

```
YYMMDD...year,month,day.
BU.......core average cycle burnup
         in MWd/MTU.
LF.......load factor in percents;
         LF=100*(daily average
         power/2300MW).
DTG......daily thermal generation in MWd.
Temp.....core average coolant temperature
         in 100°F.(e.g., 5.354 is 535.4°F).
```

Format: (X,3I2,F8.1,F7.1,F8.1,F6.3)

Fig. 1.13 Content and format of the FILE8.DAT. Beginning and end of file are shown

+213 cm (7 ft)

+107 cm (3.5 ft)

CORE MIDPLANE

-107 cm (3.5 ft)

-213 cm (7 ft)

R = 238.023 cm
(93.71 in.)
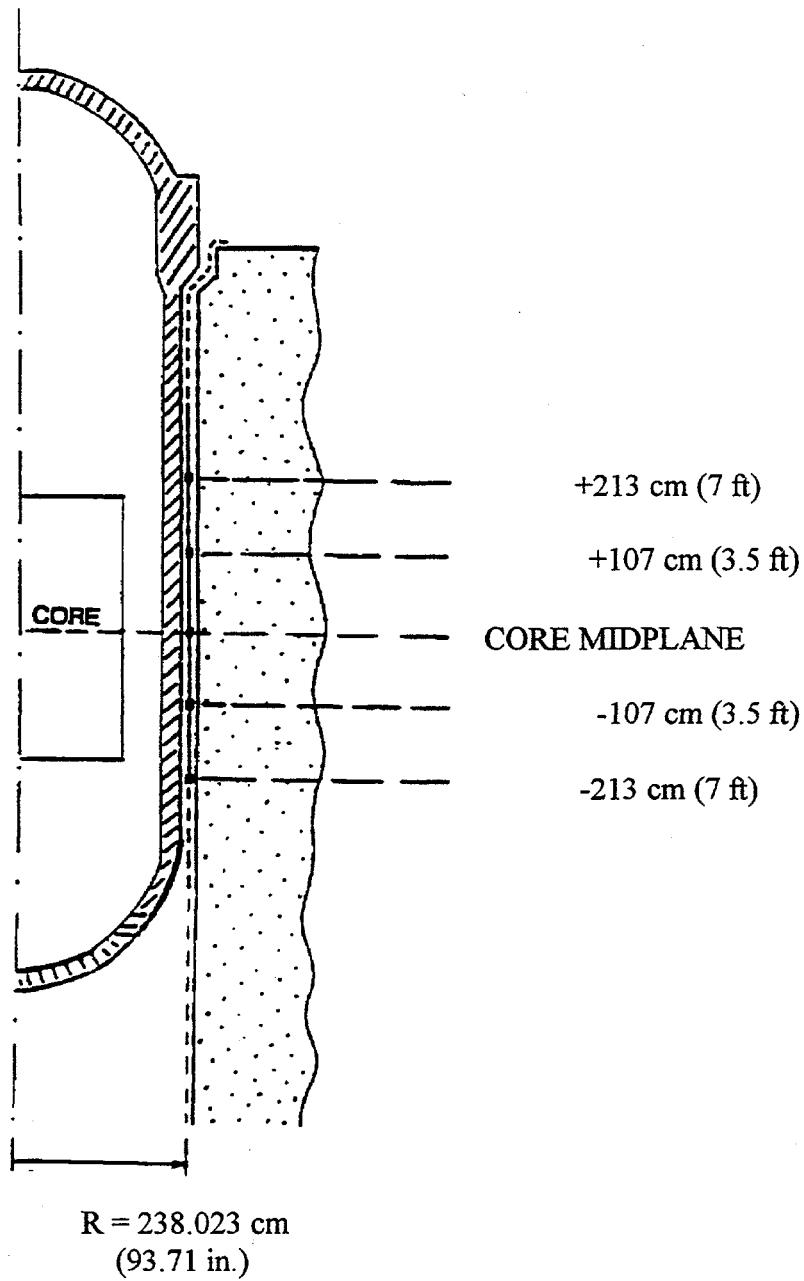
Fig. 1.14 Schematic drawing of the axial positions of the cavity dosimeters. At each of the marked locations a multiple dosimeter set was irradiated. Data in Table 1.4 are for the set in the core midplane

2 BENCHMARK ANALYSIS

2.1 METHODOLOGY

This section describes the analysis of the HBR-2 benchmark. The transport calculations were performed using the DORT computer code (Ref. 1) and the flux synthesis method.* The synthesis method, described in more detail in Ref. 2, relies on two- and one-dimensional (2-D and 1-D) transport calculations to obtain an estimation of the neutron fluxes in the three-dimensional (3-D) geometries. When the method is used to analyze a neutron field in a region outside the core of a pressurized water reactor, it calls for three transport calculations. One 2-D calculation models the horizontal cross section of the reactor in the r - θ geometry. It is used to compute the variations of the neutron field in the radial direction (which is the main direction of the neutron transport from the core toward the pressure vessel and beyond) and in the azimuthal direction. The second calculation is a 2-D calculation in cylindrical r - z geometry, in which a core is modeled as a finite-height cylinder. The third calculation is made for the 1-D (r) cylindrical model of the reactor. The r - z and 1-D r- calculations are combined to obtain the axial variations of the neutron field.

Geometry models used in this analysis were almost identical to those used in the previous HBR-2 analysis (Refs. 2, 3). The r - θ model covered one octant of the horizontal cross section with 74 azimuthal (θ) intervals. In the radial direction—which extended from the core axis to the pressure vessel, the reactor cavity and inside the concrete shield (from a radius of 0 to 345 cm)—the number of radial intervals was varied with azimuthal interval (variable mesh option) and ranged from 93 to 116 intervals. The surveillance capsule was included in the model. The r - z model used 75 axial (z-axis) intervals (57 intervals covered the active fuel height of 365.76 cm) and 93 radial intervals (from the axis of the core to the radius of 335 cm). The r - z mesh outside the core described the geometry at the azimuth of $0°$, since the benchmark cavity dosimetry is at the $0°$ azimuth. The one-dimensional calculation used the same radial mesh as the r - z model.

For the transport calculations, the cross sections of the macroscopic mixtures were prepared by the GIP code (Ref. 4), using the homogenized zone compositions given in Table 1.2 of this report. The P_3 approximation to the angular dependence of the anisotropic scattering cross sections (i.e., the P_0 to P_3 Legendre components) were taken into account, and a symmetric S_8 "directional quadrature set" (i.e., a set of discrete directions and angular quadratures) were used for all transport calculations. The benchmark was analyzed with three cross-section libraries based on ENDF/B-VI: BUGLE-93 (Ref. 5), SAILOR-95,[†] and BUGLE-96 (Ref. 6), which have 47 neutron and 20 gamma energy groups.

---

*DORT version 2.12.14, dated December 14, 1994, was used.

[†]Regarding SAILOR-95, see M. L. Williams, M. Asgari, and H. Manohara, "Letter Report on Generating SAILOR-95 Library," personal communication to F. B. K. Kam, ORNL, February 1995.

The neutron sources for the r - θ, r - z and one-dimensional calculation were prepared by the DOTSOR code.[‡] For the r - θ source, the cycle-averaged pin-power distributions in x - y geometry and cycle-average assembly powers were input into the DOTSOR, which transformed the power distribution into the r - θ geometry mesh. The power-to-neutron-source conversion factor was based on the average burnup of the peripheral assemblies (i.e., assemblies 71, 86, and 101) at the middle of cycle 9, in order to account for the contributions of ^{235}U and ^{239}Pu to the fission neutron source.[**] The source energy spectrum was taken as the average of ^{235}U and ^{239}Pu fission spectra.[††]

The source for the r - z calculation was generated by averaging the cycle-average pin powers of the top halves of the fuel elements 79 to 86 over the y axis (see Fig. 1.1; the y axis is perpendicular to the $0°$ radial direction) and multiplying the average pin-power values by the cycle-average axial power distribution of the corresponding fuel assembly. The x - z power distribution obtained was then transformed into r - z mesh by the DOTSOR code, which also prepared the source for 1-D r calculation by integrating the r - z source over the z axis. The same source energy spectrum as in the r - θ calculation was used for the r - z and r calculations.

From the three transport calculations, the neutron fluxes in the core midplane, in the surveillance capsule at the azimuth of $20°$, and in the cavity at the azimuth of $0°$ were synthesized. Reaction rates were calculated with the CROSS-95 dosimetry library (Ref. 7). The CROSS-95 cross sections were collapsed from the 640 to 47 energy groups using the FLXPRO code from the LSL-M2 code package (Ref. 8) and the reference spectra as calculated in the capsule and cavity location. The reaction rates are listed in Table 2.1.

To calculate the specific activities at the end of irradiation, which are the measured quantities provided for comparison with the calculations, it is necessary to take into account the reactor power changes during irradiation and other changes that may affect the reaction rates. As a result of fuel burnup the power distribution in the core changes gradually throughout the fuel cycle, causing changes in neutron leakage from the core and consequent changes in reaction rates at the dosimetry locations. Since the reaction rates were calculated for one power distribution only (i.e., the cycle-average power distribution) approximations are necessary to account for these gradual changes.

[‡]Regarding DOTSOR, see M. L. Williams, *DOTSOR: A Module in the LEPRICON Computer Code System for Representing the Neutron Source Distribution in LWR Cores*, EPRI Research Project 1399-1 Interim Report (December 1985), RSIC Peripheral Shielding Routine Collection PSR-277.

[**]The power-to-neutron-source conversion factor of 8.175×10^{16} neutrons $s^{-1}MW^{-1}$ was calculated by the DOTSOR code for the fuel burnup of 28596 MWd/MTU, which corresponds to the cycle-average burnup of the fuel assemblies number 71, 86, and 101.

[††]The ENDF/B-VI fission spectra for ^{235}U and ^{239}Pu were used.

Reaction rates at the dosimetry location are affected mostly by the closest fuel assemblies. Therefore, for the cavity-dosimetry location, the following approximation was used. The cycle was divided into eight time intervals, based on the burnup steps at which the power distributions were provided. That is, the first interval was taken from the beginning of cycle to the core burnup halfway between the first and second power distribution provided, the second interval from the end of the first interval to halfway between the second and third power distribution, etc. The average relative power p_i of the three fuel elements on the core flat edge (i.e., assemblies 71, 86, and 101) was calculated and assumed constant during the corresponding interval. The average relative powers (p_i) were normalized so that, when integrated over the cycle, they provide the correct total energy produced (i.e., the average energy produced in the three fuel elements, as given in FILE1.DAT). Using the daily power history, the reaction rate was then approximated as

$$R_j = R_c \times (p_i / p_{DORT}) \times (P_j / P_o),$$
(2.1)

where

R_j = reaction rate at cavity location during j-th day,

R_c = reaction rate obtained from transport (DORT) calculations, for nominal core power,

p_i = normalized average relative power of the fuel elements 71, 86, and 101 during i-th time interval,

p_{DORT} = average relative power of the fuel elements 71, 86, and 101 used in the transport calculation (DORT),

P_j = daily-average reactor core power during day j. (Day j is in the time interval i).

P_o = nominal core power (2300 MW).

The same procedure was used for the calculation of activities of the dosimeters in the surveillance capsule; however, the fuel assemblies considered were the ones closest to the capsule location— that is, assemblies 43, 56, and 71.

Different approaches can be used to account for the changes of reaction rates during the cycle; for example, one can (1) simply neglect the effects of redistribution and account only for the core power variations or (2) use the adjoint scaling techniques described in Ref. 2. The impact of different approaches on the calculated specific activities is further discussed in Appendix A.

2.2 RESULTS AND DISCUSSION

The reaction rates calculated as described in the previous subsection, for the cycle-average power distribution, are given in Table 2.1. The reaction rates obtained from the transport calculations with the BUGLE-93, SAILOR-95, and BUGLE-96 are practically identical in the surveillance capsule, for all the reactions considered; the maximum differences are less than 1%. In the cavity the reaction rates obtained by BUGLE-96 and SAILOR-95 agree to better than 1%. The reaction rates obtained by BUGLE-93 for the ^{63}Cu(n, α) and ^{46}Ti(n,p) reactions are practically identical to those obtained by the other two libraries, while BUGLE-93 reaction rates for ^{54}Fe(n,p), ^{58}Ni(n,p), ^{238}U(n,f), and ^{237}Np(n,f) are 1%, 2%, 4% and 10% lower, respectively, than reaction rates calculated with the other two libraries. These observations are consistent with the results of the Pool Critical Assembly Pressure Vessel Facility Benchmark analysis, where good agreement of the reaction rates obtained by all three libraries was found for the dosimeters located inside the pressure vessel, while in the void box behind the pressure vessel (simulating the reactor cavity), the BUGLE-93 predicted lower reaction rates than the other two libraries, for all the dosimeters except ^{237}Np, for which the BUGLE-93 predicted a higher reaction rate (Ref. 9).

Table 2.1 Reaction rates calculated for the cycle-average power distribution and core power of 2300 MW (100% of nominal power), with different cross-section libraries for transport calculations

Cross-Section Library	Reaction Rate (s^{-1} atom^{-1})					
	^{237}Np(n,f)	^{238}U(n,f)	^{58}Ni(n,p)	^{54}Fe(n,p)	^{46}Ti(n,p)	^{63}Cu(n, α)
	Capsule					
BUGLE-93	1.05E−13	1.54E−14	4.74E−15	3.50E−15	5.62E−16	3.57E−17
SAILOR-95	1.06E−13	1.55E−14	4.77E−15	3.52E−15	5.64E−16	3.58E−17
BUGLE-96	1.06E−13	1.54E−14	4.74E−15	3.51E−15	5.62E−16	3.57E−17
	Cavity					
BUGLE-93	3.72E−15	2.04E−16	4.72E−17	3.20E−17	5.16E−18	3.63E−19
SAILOR-95	4.14E−15	2.12E−16	4.82E−17	3.24E−17	5.18E−18	3.64E−19
BUGLE-96	4.13E−15	2.11E−16	4.79E−17	3.23E−17	5.16E−18	3.63E−19

With the reaction rates from Table 2.1 the specific activities were calculated as described in subsection 2.1. The calculated specific activities are given in Table 2.2. Conversion from reaction rates to specific activities does not affect the differences between results obtained by different cross-section libraries; therefore, for the comparison of specific activities the comments given above for the reaction rates apply.

Table 2.2   Calculated specific activities

Cross-Section Library	Specific activity (Bq/mg)					
	$^{237}Np(n,f)$ ^{137}Cs	$^{238}U(n,f)$ ^{137}Cs	$^{58}Ni(n,p)$ ^{58}Co	$^{54}Fe(n,p)$ ^{54}Mn	$^{46}Ti(n,p)$ ^{46}Sc	$^{63}Cu(n,\alpha)$ ^{60}Co
$T_{1/2}^{*}$	30 years	30 years	71 days	313 days	84 days	5.3 years
Capsule						
BUGLE-93	3.28E+2	4.52E+1	1.70E+4	8.68E+2	2.96E+2	2.39E+1
SAILOR-95	3.31E+2	4.56E+1	1.71E+4	8.73E+2	2.98E+2	2.40E+1
BUGLE-96	3.30E+2	4.54E+1	1.71E+4	8.69E+2	2.96E+2	2.39E+1
Cavity						
BUGLE-93	1.17E+1	6.06E−1	1.88E+2	8.27	2.99	2.47E−1
SAILOR-95	1.30E+1	6.30E−1	1.91E+2	8.36	3.00	2.47E−1
BUGLE-96	1.30E+1	6.28E−1	1.91E+2	8.32	2.99	2.47E−1

* Reaction product half-life.

Table 2.3 lists the ratios of the calculated and measured specific activities. Calculated specific activities are taken from Table 2.2. Measured specific activities are taken from Table 1.4. The average C/M ratios in the capsule, for BUGLE-93, SAILOR-95, and BUGLE-96, are 0.90 ± 0.04, 0.90 ± 0.04, and 0.90 ± 0.04, respectively. If the corrections, discussed in notes to Table 1.4, are applied to the measured activities of the ^{237}Np, ^{238}U, and ^{63}Cu dosimeters, the C/M ratios increase by ~3%, 6%, and 3% in the capsule, respectively, and by ~6%, 11%, and 3% in the cavity, respectively. The C/M ratios for the corrected measured activities are listed in Table 2.3 in parentheses.

Table 2.3   Ratios of calculated-to-measured (C/M) specific activities*

Cross-Section Library	^{237}Np(n,f) ^{137}Cs	^{238}U(n,f) ^{137}Cs	^{58}Ni(n,p) ^{58}Co	^{54}Fe(n,p) ^{54}Mn	^{46}Ti(n,p) ^{46}Sc	^{63}Cu(n,α) ^{60}Co	Average†
$T_{1/2}$‡	30 years	30 years	71 days	313 days	84 days	5.3 years	
Capsule							
BUGLE-93	0.89 (0.92)	0.85 (0.89)	0.95	0.93	0.85	0.90 (0.93)	0.90 ± 0.04 (0.91 ± 0.04)
SAILOR-95	0.90 (0.92)	0.85 (0.90)	0.96	0.93	0.85	0.91 (0.93)	0.90 ± 0.04 (0.92 ± 0.04)
BUGLE-96	0.90 (0.92)	0.85 (0.89)	0.96	0.93	0.85	0.90 (0.93)	0.90 ± 0.04 (0.91 ± 0.04)
Cavity							
BUGLE-93	0.52 (0.55)	0.71 (0.79)	0.96	0.95	0.90	0.93 (0.96)	0.89 ± 0.10 (0.91 ± 0.07)
SAILOR-95	0.58 (0.61)	0.74 (0.82)	0.98	0.96	0.91	0.94 (0.96)	0.91 ± 0.10 (0.93 ± 0.06)
BUGLE-96	0.58 (0.61)	0.74 (0.82)	0.97	0.96	0.90	0.93 (0.96)	0.90 ± 0.09 (0.92 ± 0.06)

* Ratios C/M are given for the as-measured specific activities. The ratios given in parentheses are calculated with corrections, specified in Table 1.4, applied to ^{237}Np(n,f)^{137}Cs, ^{238}U(n,f)^{137}Cs, and ^{63}Cu(n,α)^{60}Co measured reaction rates.

† Average C/M ratio and standard deviation. For the cavity location averages are calculated without ^{237}Np(n,f)^{137}Cs reaction. The averages with ^{237}Np(n,f)^{137}Cs reaction are 0.83 ± 0.18 (0.85 ± 0.16), 0.85 ± 0.16 (0.87 ± 0.14), and 0.85 ± 0.16 (0.87 ± 0.14), for BUGLE-93, SAILOR-95, and BUGLE-96 libraries, respectively. Values in parentheses are calculated with corrections applied to ^{237}Np, ^{238}U, and ^{63}Cu dosimeters, as discussed in the footnote above.

‡ Reaction product half-life.

In the cavity the C/M ratio for the ^{237}Np dosimeter is significantly lower than C/M ratios for other dosimeters, regardless of the cross-section library used.* Therefore, the average C/M values in the cavity, given in Table 2.3 in the last column on the right, were calculated without the Np dosimeter.

---

*This well-known problem of the HBR-2 cycle 9 cavity dosimetry measurements was addressed in several analyses, but has not been completely explained. Currently the most probable explanation appears to be an incorrect measured value.

The average C/M values in the cavity for BUGLE-93, SAILOR-95, and BUGLE-96 are 0.89 ± 0.10, 0.91 ± 0.10, and 0.90 ± 0.09, respectively.[†] The C/M ratios given in parentheses are for the measured activities of ^{237}Np, ^{238}U, and ^{63}Cu dosimeters, corrected as discussed in notes to Table 1.4. The average C/M ratios in the cavity are practically identical to those in the capsule; therefore, no decrease in the C/M ratios with increasing distance from the core and increasing thickness of steel penetrated is observed. Such decrease was typical for the pre-ENDF/B-VI cross-section libraries and is illustrated in Appendix A.

The variations of the C/M values for different dosimeters at the same location are small: the standard deviation of the average C/M ratios is ~0.04 in the capsule and ~0.10 in the cavity.[‡] These values suggest that the shapes of the calculated spectra, in the energy range to which the measured dosimeters are sensitive, are adequate. To further assess the differences between the three libraries the calculated multigroup neutron spectra are tabulated and compared in Appendix B. The tabulated spectra were used to determine the reaction rates given in Table 2.1. In the capsule the multigroup fluxes calculated with the BUGLE-93, SAILOR-95, and BUGLE-96 libraries agree to within ~2%, except at thermal energies where differences are bigger: below ~0.1eV SAILOR-95 and BUGLE-93 predicted, respectively, ~2 times lower and 2.7 times higher flux than BUGLE-96 (see Fig. B.2). These differences at the low energies are not important for predicting radiation damage in the steel specimens and reaction rates of the threshold neutron dosimeters in the capsule.

In the cavity, the group fluxes calculated with the SAILOR-95 and BUGLE-96 libraries agree to better than 1% over the entire energy range while the BUGLE-93 fluxes differ considerably (see Fig. B.4). BUGLE-93 predicted up to two times higher fluxes below 1eV, and, more importantly, lower fluxes at higher energies, except between ~10keV and 70keV. Between ~0.1MeV and 2MeV, BUGLE-93 predicted at least 5% lower fluxes than BUGLE-96, with the maximum difference about 18% at ~0.7 MeV. This comparison, combined with the observation that the calculations underpredicted the reaction rates, suggests that neutron flux and spectrum in the cavity are more accurately predicted by the BUGLE-96 library than by the BUGLE-93 library. Some support for this suggestion can also be found from the comparison of the calculated and measured specific activities (see Table 2.3). In the cavity, the BUGLE-93 library gave slightly lower C/M ratios than the other two libraries for the ^{58}Ni dosimeter and in particular for the ^{238}U and ^{237}Np dosimeters, which have lower reaction energy thresholds and are sensitive to the neutrons below ~2MeV. Similar differences, as observed here between the multigroup fluxes calculated by the BUGLE-93 and BUGLE-96 libraries, were also found in the analysis of the Pool Critical Assembly Pressure Vessel Facility (Ref. 9).

[†] If the ^{237}Np dosimeter in the cavity is taken into account, the average C/M values are 0.83 ± 0.18, 0.85 ± 0.16, and 0.85 ± 0.16, for the BUGLE-93, SAILOR-95, and BUGLE-96 library, respectively.

[‡] If the ^{237}Np dosimeter in the cavity is taken into account, the standard deviation of the average C/M is ~0.16.

2.3 REFERENCES

1. W. A. Rhoades et al., "TORT-DORT Two- and Three-Dimensional Discrete Ordinates Transport, Version 2.8.14," CCC-543, Radiation Shielding Information Center, Oak Ridge National Laboratory, 1994.

2. R. E. Maerker, "LEPRICON Analysis of the Pressure Vessel Surveillance Dosimetry Inserted into H. B. Robinson-2 During Cycle 9," *Nuc. Sci. Eng.*, 96:263 (1987).

3. M. L. Williams, M. Asgari, F. B. K. Kam, *Impact of ENDF/B-VI Cross-Section Data on H. B. Robinson Cycle 9 Dosimetry Calculations*, NUREG/CR-6071 (ORNL/TM-12406), October 1993.

4. W. A. Rhoades, "The GIP Program for Preparation of Group-Organized Cross-Section Libraries," informal notes, November 1975, RSIC Peripheral Shielding Routine Collection PSR-75.

5. D. T. Ingersoll et al., "Bugle-93: Coupled 47 Neutron, 20 Gamma-Ray Group Cross-Section Library Derived from ENDF/B-VI for LWR Shielding and Pressure Vessel Dosimetry Applications," RSIC Data Library Collection, DLC-175, February 1994.

6. J. E. White et al., "BUGLE-96: Coupled 47 Neutron, 20 Gamma-Ray Group Cross Section Library Derived from ENDF/B-VI for LWR Shielding and Pressure Vessel Dosimetry Applications," RSIC Data Library Collection, DLC-185, March 1996.

7. I. Remec and F. B. K. Kam, *An Update of the Dosimetry Cross-Section Data Base for the Adjustment Code LSL-M2*, ORNL/NRC/LTR-95/20, June 1995.

8. F. W. Stallmann, *LSL-M2: A Computer Program for Least-Squares Logarithmic Adjustment of Neutron Spectra*, NUREG/CR-4349 (ORNL/TM-9933), March 1986.

9. I. Remec and F. B. K. Kam, *Pool Critical Assembly Pressure Vessel Facility Benchmark*, NUREG/CR-6454 (ORNL/TM-13205), July 1997.

3 CONCLUSIONS

Section 1 of this report describes the HBR-2 pressure vessel dosimetry benchmark and provides all the dimensions, material compositions and neutron source data necessary for the analysis. The neutron source data are provided on the floppy disk accompanying this report.

In Section 2, the analysis of the HBR-2 benchmark is presented. The transport calculations with the computer code DORT, based on the discrete-ordinates method, were performed with three ENDF/B-VI-based multigroup libraries: BUGLE-93, SAILOR-95, and BUGLE-96. Excellent agreement of the calculated specific activities with the measurements was obtained. For the dosimeters in the surveillance capsule, the average C/M ratios for BUGLE-93, SAILOR-95, and BUGLE-96, are 0.90 ± 0.04, 0.90 ± 0.04, and 0.90 ± 0.04, respectively. For the dosimeters irradiated in the cavity, the average C/M ratios (excluding ^{237}Np dosimeter) for BUGLE-93, SAILOR-95, and BUGLE-96, are 0.89 ± 0.10, 0.91 ± 0.10, and 0.90 ± 0.09, respectively. The C/M ratios given above are for the as-measured specific activities (e.g., no corrections were applied to the ^{237}Np, ^{238}U, and ^{63}Cu dosimeters). No systematic decrease in the C/M ratios with increasing distance from the core was observed for any of the libraries used.

It is expected that the agreements of the calculations with the measurements, similar to those shown in this report, should typically be obtained when the discrete-ordinates method and the ENDF/B-VI cross-section libraries are used for the HBR-2 benchmark analysis.

APPENDIX A

COMPARISON OF APPROXIMATIONS FOR MODELING THE REACTION RATE VARIATIONS DUE TO CORE POWER REDISTRIBUTION AND COMPARISON OF RESULTS OBTAINED WITH ENDF/B-IV AND ENDF/B-VI CROSS SECTIONS
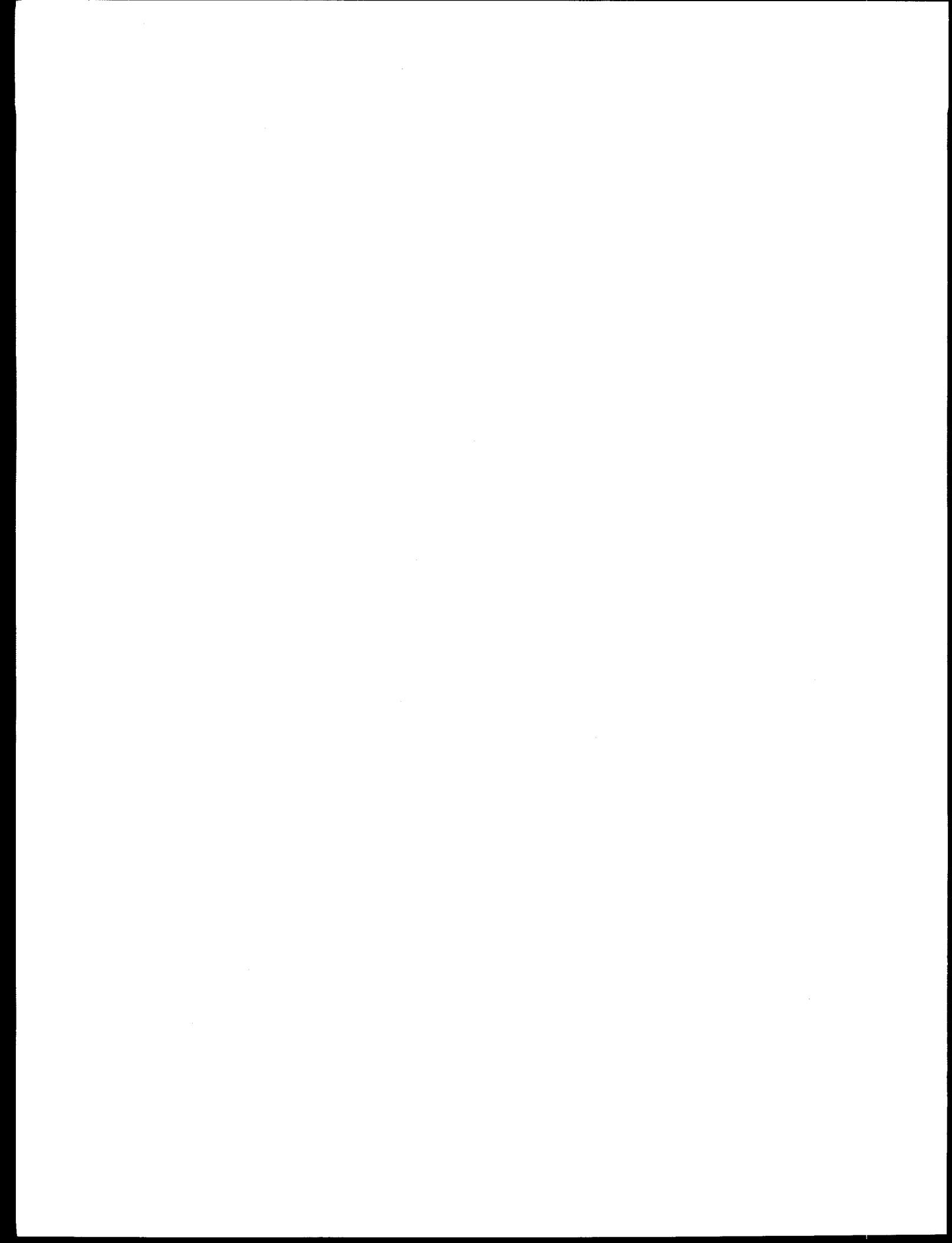
In the steady-state neutron field the activities of the dosimeters during irradiation gradually approach the saturated activities, which are proportional to the reaction rates. For a given dosimeter and reaction rate, the activity of the dosimeter depends only on the time of irradiation. The transformation of the measured specific activity into the reaction rate is simple; it does not involve approximations and it does not introduce uncertainties other than those related to the characteristics of the dosimeter and reaction product. Therefore, the reaction rates deduced from activities measured in a steady-state neutron field are usually referred to as "measured" reaction rates.

However, in a power reactor the neutron field and consequently the reaction rates vary with time because (1) the power distribution in the core gradually changes with fuel burnup ("power-redistribution") and (2) the changes of the reactor power. The reaction rates are often calculated for a given core condition only (e.g., nominal thermal power, at certain core burnup), and approximations are necessary in the calculation of specific activities. To approximate the effect of the changes of the core power it is usually assumed that the reaction rates are proportional to the core power (at all locations of the dosimeters). The changes in reaction rates caused by the power redistribution may vary from negligible to ~30 to 40%. These changes depend primarily on the fuel loading pattern (and, therefore, vary from cycle to cycle) and may be different for different dosimetry locations. Since the treatment of the power-redistribution effect is less standardized, the effect of a few different approximations is illustrated on the example of HBR-2 cycle 9 dosimetry analysis. The following approaches were considered:

(a) Changes due to redistribution were approximately accounted for as described insubsection 2.1 [e.g., the reaction rates were taken proportional to the core power (daily-averaged) and average relative power of the fuel assemblies closest to the location of the dosimeters].

(b) The redistribution effect was neglected, and reaction rates were taken proportional to the core power (daily-averaged).

(c) Reaction rates from the present analysis were converted into the specific activities by the conversion factors determined from Ref. 1. In Ref. 1 the adjoint scaling technique was used to determine the reaction rates for eight core power distributions during the cycle and then the specific activities were calculated by superimposing the power history. This method should be more accurate than the two approaches described above. However, in Ref. 1 the core power distributions from an older analysis were used, which may affect the reaction-rate-to-activity conversion factors and consequently the comparison with the results from steps (a) and (b).

Using the reaction rates obtained from the transport calculation with the BUGLE-96 library, the specific activities were calculated according to the three approximations described above. The C/M ratios for the capsule and cavity dosimeters are listed in Table A.1. In the capsule the three approximations give very similar average C/M ratios and corresponding standard deviations. This similarity exists because the changes of the power of the peripheral fuel assemblies closest to the capsule are relatively small; the average power of the elements number 43, 56, and 71 increased only ~20% from the beginning to the end of cycle. However, the average power of the assemblies on the

flat edge (i.e., assemblies 71, 86 and 101) increased over 60% from the beginning to the end of the cycle, and this power increase affects the comparisons in the cavity. Approximations (a), (b), and (c) gave the average C/M values in the cavity of 0.90 ± 0.09, 0.83 ± 0.08, and 0.84 ± 0.08, respectively. The advantage of approximation (a) over (b) is clearly shown. The largest differences in the C/M ratios are observed for the reactions with short-lived products, $^{58}Ni(n,p)^{58}Co$ and $^{46}Ti(n,p)^{46}Sc$; the C/M for the fission dosimeters, for which the activity of long-lived ^{137}Cs is measured, are almost unaffected. The approximations (b) and (c) give very similar results: average C/M and its standard deviation in the cavity are 0.83 ± 0.08, and 0.84 ± 0.08, respectively, and in the capsule are 0.88 ± 0.04, and 0.89 ± 0.05, respectively. Therefore, in this case it appears that using the adjoint scaling technique [i.e., approximation (c)] gives little advantage over the simpler approximation (b),which accounts for core power variations only. However, the application of conversion factors, calculated from results obtained by adjoint scaling in Ref. 1, to the reaction rates calculated in the present analysis, is approximate, as described above.

The HBR-2 cycle 9 dosimetry has been analyzed before; see for example Refs. 1 and 2. In Ref. 1, ELXSIR cross sections (Ref. 3) based on ENDF/B-IV were used. In Ref. 2, SAILOR cross sections (Ref. 4) based on ENDF/B-IV with iron, oxygen, and hydrogen cross sections from the ENDF/B-VI library and ENDF/B-VI dosimetry cross sections were used. To assess the impact of the ENDF/B-VI-based cross-section library for transport calculations, the analysis was repeated with exactly the same neutron source (i. e., spatial power distribution in the core, and source energy spectrum between ^{235}U and ^{239}Pu ENDF/B-V fission spectra) and modeling approximations that were used in Refs. 1 and 2. For consistency (with Refs. 1 and 2), the time-dependent variations of reaction rates were approximated by using the mid-cycle reaction rates to the end-of-cycle activities conversion factors from Ref. 1, and the measured reaction rates were corrected as described in the note to Table 1.4. The SAILOR-95 (ENDF/B-VI-based) cross sections for transport calculations were used, and dosimetry cross sections were taken from CROSS-95. This analysis will be referred to in the following discussion as the "new" analysis. The C/M ratios for the capsule and cavity dosimeters from the new analysis are compared with the values from Refs. 1 and 2 in Table A.2.

In the capsule, the new analysis gave the average C/M of 0.93 ± 0.05, slightly lower than the average of 0.96 ± 0.05 from Ref. 2. This lower value is present probably because in the new analysis and in Ref. 2 the reaction rates inside the capsule were determined at slightly different radial locations. Both Ref. 2 and the new analysis gave significantly improved C/M values over the values from Ref. 1: the increase in the average C/M in the capsule is ~12% for the new analysis and ~16% for the Ref. 2.

In the cavity location, the new analysis and Ref. 2 gave practically identical results, with the average C/M of 0.88 ± 0.14, while the C/M average for the Ref. 1 is 0.66 ± 0.04. Therefore, the increase in the average C/M ratio is ~33%. For the $^{237}Np(n,f)^{137}Cs$ reaction the C/M ratio in the new analysis and in Ref. 2 is about 0.61 and differs significantly from the C/M ratios for the other dosimeters, as can be seen from Table A.2. The average C/M for the cavity location calculated without the $^{237}Np(n,f)^{137}Cs$ reaction is 0.93 for the new analysis and Ref. 2, and 0.67 for Ref. 1; therefore, an improvement of 39% was obtained.

The ENDF/B-VI-based cross sections for transport calculations resulted in improved agreement of calculations and measurements, both in the capsule and in the cavity. The average C/M in the capsule, for the six dosimeters used, is ~0.93 ± 0.05; the ENDF/B-IV-based library gave 0.83 ± 0.03. In the cavity, the average (excluding ^{237}Np dosimeter) is 0.93 ± 0.06, and 0.67 ± 0.03 for the ENDF/B-VI- and ENDF/B-IV-based libraries, respectively. Therefore, the ENDF/B-VI-based cross sections eliminated the decrease of the C/M ratios with increasing distance from the core and increasing thickness of the steel penetrated by neutrons.

Table A.1 Ratios of calculated-to-measured (C/M) specific activities obtained with different approximations for the time-dependent variations of reaction rates*

	^{237}Np(n,f) ^{137}Cs	^{238}U(n,f) ^{137}Cs	^{58}Ni(n,p) ^{58}Co	^{54}Fe(n,p) ^{54}Mn	^{46}Ti(n,p) ^{46}Sc	^{63}Cu(n,α) ^{60}Co	Average[†]
$T_{1/2}$[‡]	30 years	30 years	71 days	313 days	84 days	5.3 years	
Capsule							
Approx. (a)**	0.90 (0.92)	0.85 (0.89)	0.96	0.93	0.85	0.90 (0.93)	0.90 ± 0.04 (0.91 ± 0.04)
Approx. (b)**	0.90 (0.92)	0.85 (0.89)	0.90	0.91	0.80	0.90 (0.92)	0.88 ± 0.04 (0.89 ± 0.05)
Approx. (c)**	0.86 (0.88)	0.82 (0.86)	0.98	0.91	0.87	0.87 (0.89)	0.89 ± 0.05 (0.90 ± 0.04)
Cavity							
Approx. (a)**	0.58 (0.61)	0.74 (0.82)	0.97	0.96	0.90	0.93 (0.96)	0.90 ± 0.09 (0.92 ± 0.06)
Approx. (b)**	0.57 (0.60)	0.73 (0.80)	0.83	0.90	0.78	0.92 (0.94)	0.83 ± 0.08 (0.85 ± 0.07)
Approx. (c)**	0.55 (0.57)	0.70 (0.77)	0.90	0.90	0.84	0.88 (0.91)	0.84 ± 0.08 (0.86 ± 0.06)

* Ratios C/M are given for the as-measured specific activities. The ratios given in parentheses are calculated with corrections, specified in Table 1.4, applied to ^{237}Np(n,f)^{137}Cs, ^{238}U(n,f)^{137}Cs, and ^{63}Cu(n,α)^{60}Co measured reaction rates.

[†] Average C/M ratio and standard deviation. For the cavity location, averages are calculated without ^{237}Np(n,f)^{137}Cs reaction. The averages with ^{237}Np(n,f)^{137}Cs reaction are 0.85 ± 0.16 (0.87 ± 0.14), 0.79 ± 0.13 (0.81 ± 0.12), and 0.80 ± 0.14 (0.82 ± 0.13), for methods (a), (b), and (c), respectively. Values in parentheses are calculated with corrections applied to ^{237}Np, ^{238}U, and ^{63}Cu dosimeters, as discussed in the footnote above.

[‡] Reaction product half-life.

** See text for the explanation of the approximations (a), (b), and (c).

Table A.2 Comparison of the C/M ratios of specific activities from the present analysis with the values from the previous analyses (Refs. 1 and 2)

	C/M ratios						
	^{237}Np(*n,f*) ^{137}Cs	^{238}U(*n,f*) ^{137}Cs	^{58}Ni(*n,p*) ^{58}Co	^{54}Fe(*n,p*) ^{54}Mn	^{46}Ti(*n,p*) ^{46}Sc	^{63}Cu(*n,α*) ^{60}Co	Average C/M ±σ
Capsule							
New Analysis*	0.91	0.89	1.01	0.95	0.89	0.91	0.93 ± 0.05
Analysis from Ref. 1[†]	0.85	0.80	0.87	0.83	0.81	0.83	0.83 ± 0.03
Analysis from Ref. 2[‡]	0.94	0.93	1.05	0.98	0.92	0.95	0.96 ± 0.05
Cavity							
New Analysis*	0.62	0.84	0.98	0.97	0.89	0.95	0.88 ± 0.14 (0.93 ± 0.06)**
Analysis from Ref. 1[†]	0.61	0.65	0.66	0.68	0.66	0.72	0.66 ± 0.04 (0.67 ±0.03)**
Analysis from Ref. 2[‡]	0.61	0.86	0.97	0.97	0.90	0.96	0.88 ± 0.14 (0.93 ± 0.05)**

*   New analysis, using SAILOR-95 and CROSS-95 cross sections.

[†]   Results from Ref. 1, using ELXSIR cross sections, based on ENDF/B-IV.

[‡]   Results from Ref. 2, using SAILOR cross sections (based on ENDF/B-IV) with iron, oxygen, and hydrogen cross sections from ENDF/B-VI library and ENDF/B-VI dosimetry cross-sections.

**   C/M for neptunium omitted from the average.

APPENDIX A REFERENCES

1.   R. E. Maerker, "LEPRICON Analysis of the Pressure Vessel Surveillance Dosimetry Inserted into H. B. Robinson-2 During Cycle 9," *Nuc. Sci. Eng.*, 96:263 (1987).

2.   M. L. Williams, M. Asgari, F. B. K. Kam, *Impact of ENDF/B-VI Cross-Section Data on H. B. Robinson Cycle 9 Dosimetry Calculations*, NUREG/CR-6071 (ORNL/TM-12406), October 1993.

3.   M. L. Williams et al., *The ELXSIR Cross-Section Library for LWR Pressure Vessel Irradiation Studies: Part of the LEPRICON Computer Code System*, EPRI NP-3654, Electric Power Research Institute, Palo Alto, Calif.,1984.

4.   G. L. Simmons and R. W. Roussin, "SAILOR- Coupled, Self-Shielded, 47 Neutron, 20 Gamma-Ray, P_3, Cross-Section Library for Light Water Reactors," DLC-76, Radiation Shielding Information Center, Oak Ridge National Laboratory, 1985.

APPENDIX B

CALCULATED NEUTRON SPECTRA AT THE DOSIMETRY LOCATIONS
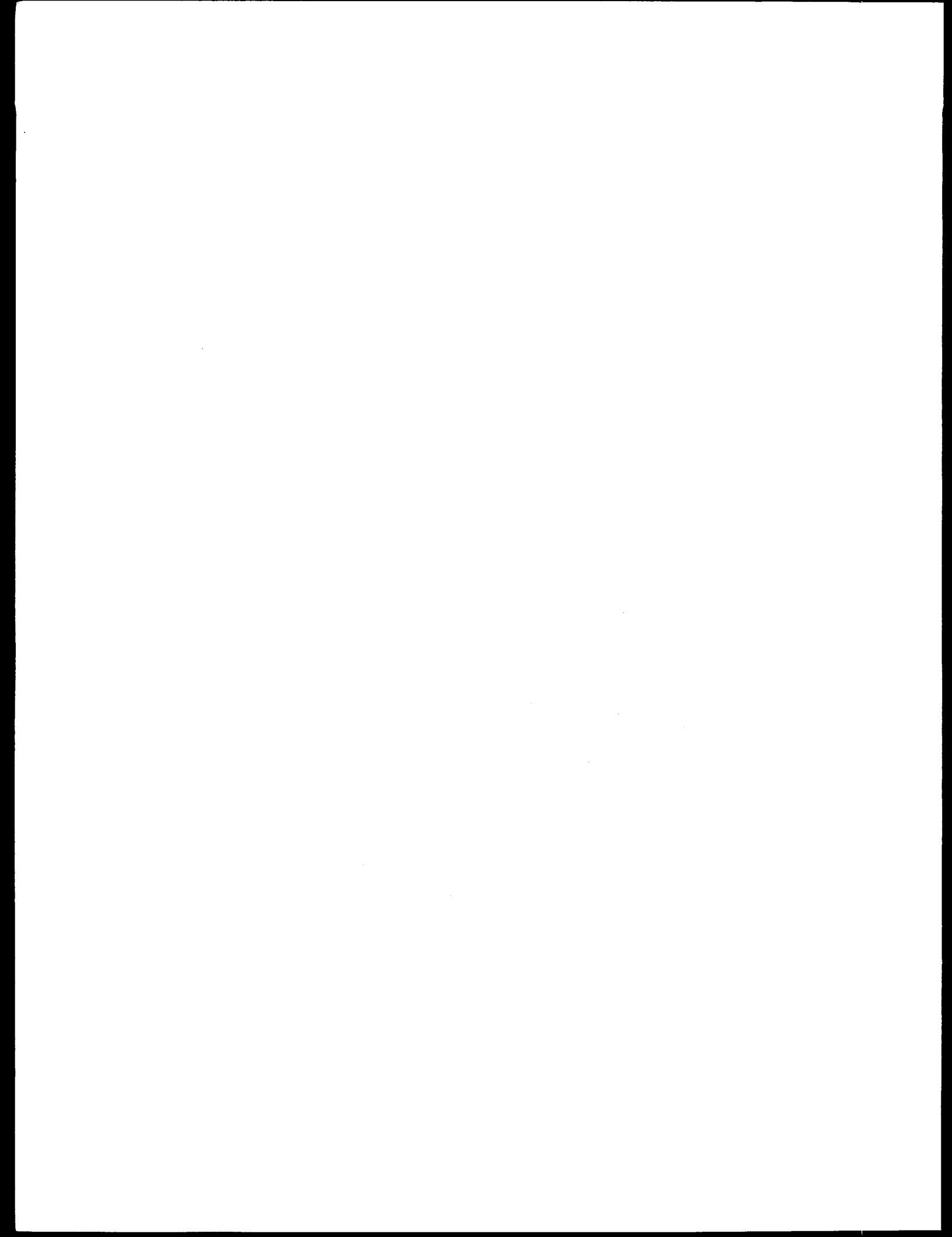
Table B.1 Calculated multigroup neutron fluxes in the surveillance capsule (20° azimuth, core midplane, at the radius of 191.15 cm from core vertical axis)

Group number	Group upper energy limit	Neutron flux		
		BUGLE-93	SAILOR-95	BUGLE-96
	eV	$cm^{-2} s^{-1}$	$cm^{-2} s^{-1}$	$cm^{-2} s^{-1}$
1	1.733E+07	8.870E+06	8.870E+06	8.870E+06
2	1.419E+07	2.808E+07	2.808E+07	2.808E+07
3	1.221E+07	1.207E+08	1.207E+08	1.207E+08
4	1.000E+07	2.379E+08	2.379E+08	2.379E+08
5	8.607E+06	4.113E+08	4.117E+08	4.112E+08
6	7.408E+06	9.984E+08	1.001E+09	9.984E+08
7	6.065E+06	1.485E+09	1.493E+09	1.485E+09
8	4.966E+06	2.865E+09	2.891E+09	2.866E+09
9	3.679E+06	2.219E+09	2.229E+09	2.220E+09
10	3.012E+06	1.710E+09	1.719E+09	1.713E+09
11	2.725E+06	1.998E+09	2.005E+09	2.001E+09
12	2.466E+06	9.928E+08	9.989E+08	9.963E+08
13	2.365E+06	2.768E+08	2.786E+08	2.779E+08
14	2.346E+06	1.383E+09	1.392E+09	1.388E+09
15	2.231E+06	3.767E+09	3.790E+09	3.780E+09
16	1.920E+06	4.382E+09	4.427E+09	4.411E+09
17	1.653E+06	6.576E+09	6.664E+09	6.633E+09
18	1.353E+06	1.190E+10	1.207E+10	1.203E+10
19	1.003E+06	8.127E+09	8.258E+09	8.228E+09
20	8.208E+05	4.085E+09	4.147E+09	4.136E+09
21	7.427E+05	1.150E+10	1.180E+10	1.176E+10
22	6.081E+05	9.276E+09	9.333E+09	9.306E+09
23	4.979E+05	1.001E+10	1.040E+10	1.035E+10
24	3.688E+05	9.367E+09	9.430E+09	9.409E+09
25	2.972E+05	1.284E+10	1.319E+10	1.316E+10
26	1.832E+05	1.177E+10	1.185E+10	1.181E+10
27	1.111E+05	8.987E+09	9.102E+09	9.076E+09
28	6.738E+04	7.444E+09	7.496E+09	7.473E+09
29	4.087E+04	2.752E+09	2.796E+09	2.790E+09
30	3.183E+04	1.316E+09	1.432E+09	1.429E+09

Table B.1 (continued)

Group number	Group upper energy limit	Neutron flux		
		BUGLE-93	SAILOR-95	BUGLE-96
	eV	cm^{-2} s^{-1}	cm^{-2} s^{-1}	cm^{-2} s^{-1}
31	2.606E+04	2.557E+09	2.578E+09	2.571E+09
32	2.418E+04	1.539E+09	1.552E+09	1.546E+09
33	2.188E+04	3.961E+09	4.038E+09	4.027E+09
34	1.503E+04	7.440E+09	7.589E+09	7.550E+09
35	7.102E+03	8.556E+09	8.686E+09	8.663E+09
36	3.355E+03	7.928E+09	8.047E+09	8.024E+09
37	1.585E+03	1.302E+10	1.332E+10	1.328E+10
38	4.540E+02	7.223E+09	7.381E+09	7.362E+09
39	2.144E+02	7.900E+09	8.050E+09	8.031E+09
40	1.013E+02	1.037E+10	1.056E+10	1.053E+10
41	3.727E+01	1.265E+10	1.288E+10	1.284E+10
42	1.068E+01	7.259E+09	7.383E+09	7.365E+09
43	5.043E+00	9.579E+09	9.360E+09	9.384E+09
44	1.855E+00	7.103E+09	6.297E+09	6.357E+09
45	8.764E-01	6.081E+09	4.893E+09	4.933E+09
46	4.140E-01	1.268E+10	7.068E+09	7.074E+09
47	1.000E-01	2.709E+10	5.339E+09	9.820E+09
	1.000E-05*			

* Low-energy boundary of the last group.

TABLE B.2 Calculated multigroup neutron fluxes at the location of cavity dosimeters (0° azimuth, core midplane, at the radius of 238.02 cm from core vertical axes)

Group number	Group upper energy limit	Neutron flux		
		BUGLE-93	SAILOR-95	BUGLE-96
	eV	$cm^{-2}s^{-1}$	$cm^{-2}s^{-1}$	$cm^{-2}s^{-1}$
1	1.733E+07	1.385E+05	1.386E+05	1.386E+05
2	1.419E+07	3.917E+05	3.915E+05	3.918E+05
3	1.221E+07	1.544E+06	1.544E+06	1.545E+06
4	1.000E+07	2.828E+06	2.827E+06	2.827E+06
5	8.607E+06	4.247E+06	4.251E+06	4.248E+06
6	7.408E+06	8.486E+06	8.507E+06	8.487E+06
7	6.065E+06	1.185E+07	1.190E+07	1.185E+07
8	4.966E+06	2.262E+07	2.284E+07	2.265E+07
9	3.679E+06	1.910E+07	1.929E+07	1.918E+07
10	3.012E+06	1.572E+07	1.594E+07	1.585E+07
11	2.725E+06	1.992E+07	2.020E+07	2.012E+07
12	2.466E+06	1.051E+07	1.075E+07	1.071E+07
13	2.365E+06	3.397E+06	3.494E+06	3.480E+06
14	2.346E+06	1.736E+07	1.788E+07	1.782E+07
15	2.231E+06	4.876E+07	5.011E+07	4.996E+07
16	1.920E+06	7.343E+07	7.712E+07	7.683E+07
17	1.653E+06	1.291E+08	1.379E+08	1.373E+08
18	1.353E+06	3.391E+08	3.705E+08	3.694E+08
19	1.003E+06	3.610E+08	3.967E+08	3.952E+08
20	8.208E+05	1.607E+08	1.745E+08	1.740E+08
21	7.427E+05	8.500E+08	1.038E+09	1.034E+09
22	6.081E+05	8.319E+08	8.919E+08	8.884E+08
23	4.979E+05	8.257E+08	9.839E+08	9.820E+08
24	3.688E+05	1.350E+09	1.609E+09	1.604E+09
25	2.972E+05	1.530E+09	1.692E+09	1.694E+09
26	1.832E+05	1.726E+09	1.870E+09	1.862E+09
27	1.111E+05	1.120E+09	1.150E+09	1.147E+09
28	6.738E+04	8.178E+08	7.908E+08	7.871E+08
29	4.087E+04	2.591E+08	2.583E+08	2.574E+08
30	3.183E+04	1.546E+08	1.613E+08	1.607E+08

Table B.2 (continued)

Group number	Group upper energy limit	Neutron flux		
		BUGLE-93	SAILOR-95	BUGLE-96
	eV	$cm^{-2} s^{-1}$	$cm^{-2} s^{-1}$	$cm^{-2} s^{-1}$
31	2.606E+04	5.410E+08	5.322E+08	5.319E+08
32	2.418E+04	3.489E+08	3.299E+08	3.285E+08
33	2.188E+04	5.325E+08	5.175E+08	5.163E+08
34	1.503E+04	6.552E+08	6.657E+08	6.612E+08
35	7.102E+03	6.656E+08	6.775E+08	6.739E+08
36	3.355E+03	5.392E+08	5.508E+08.	5.480E+08
37	1.585E+03	7.867E+08	8.201E+08	8.160E+08
38	4.540E+02	3.945E+08	4.130E+08	4.112E+08
39	2.144E+02	3.872E+08	4.057E+08	4.041E+08
40	1.013E+02	4.742E+08	4.975E+08	4.957E+08
41	3.727E+01	5.282E+08	5.547E+08	5.529E+08
42	1.068E+01	2.813E+08	2.955E+08	2.946E+08
43	5.043E+00	3.373E+08	3.392E+08	3.385E+08
44	1.855E+00	2.306E+08	2.133E+08	2.135E+08
45	8.764E-01	1.836E+08	1.692E+08	1.692E+08
46	4.140E-01	3.610E+08	2.124E+08	2.123E+08
47	1.000E-01	8.827E+08	4.383E+08	4.397E+08
	1.000E-05[*]			

[*] Low-energy boundary of the last group.
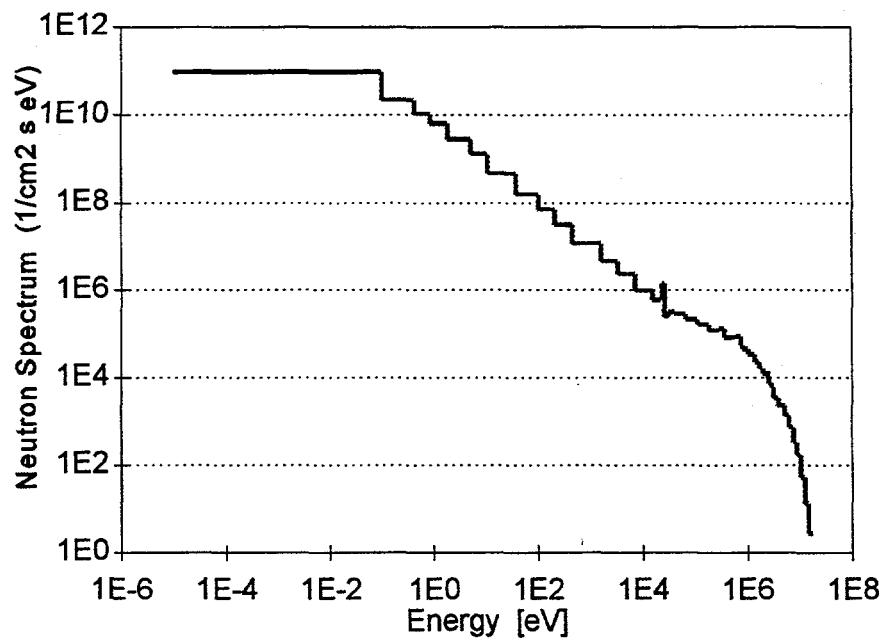
Fig. B.1 Multigroup neutron spectrum, calculated with BUGLE-96 library, in the surveillance capsule (20° azimuth, core midplane, at the radius of 191.15 cm from core vertical axis)
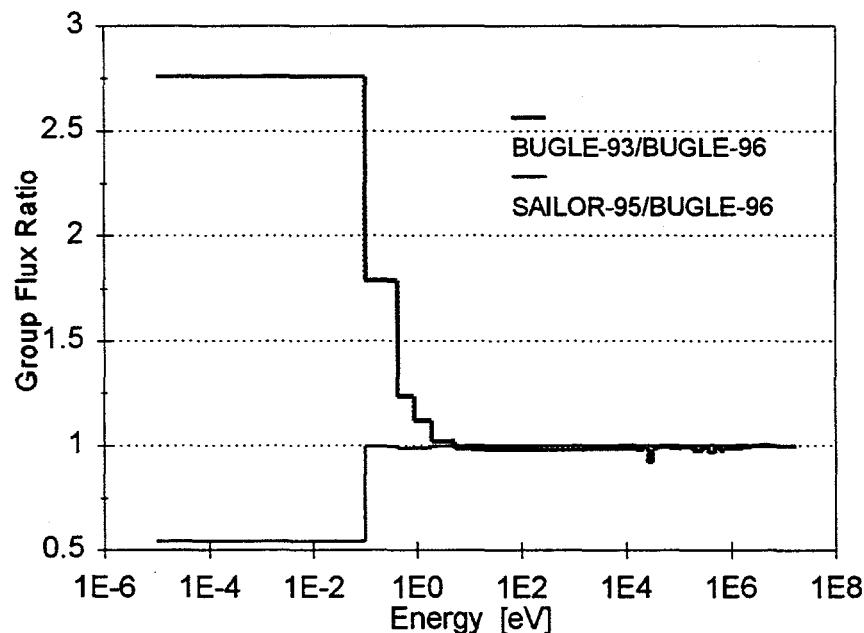

Fig. B.2 Comparison of multigroup neutron spectra, calculated with different cross-section libraries, in the surveillance capsule (20° azimuth, core midplane, at the radius of 191.15 cm from core vertical axis)
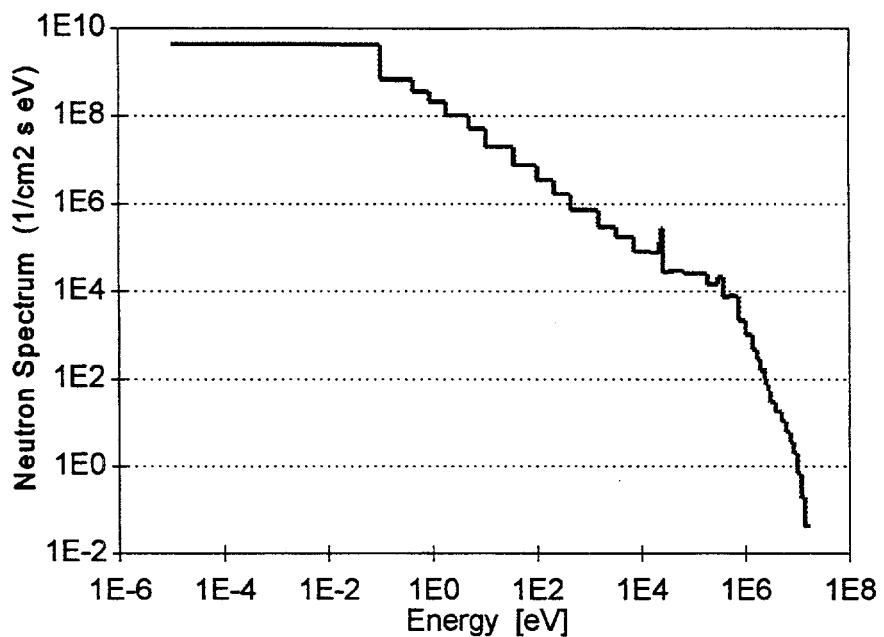
Fig. B.3 Multigroup neutron spectrum, calculated with BUGLE-96 library, at the position of cavity dosimeters (0°azimuth, core midplane, at the radius of 238.02 cm from core vertical axis)
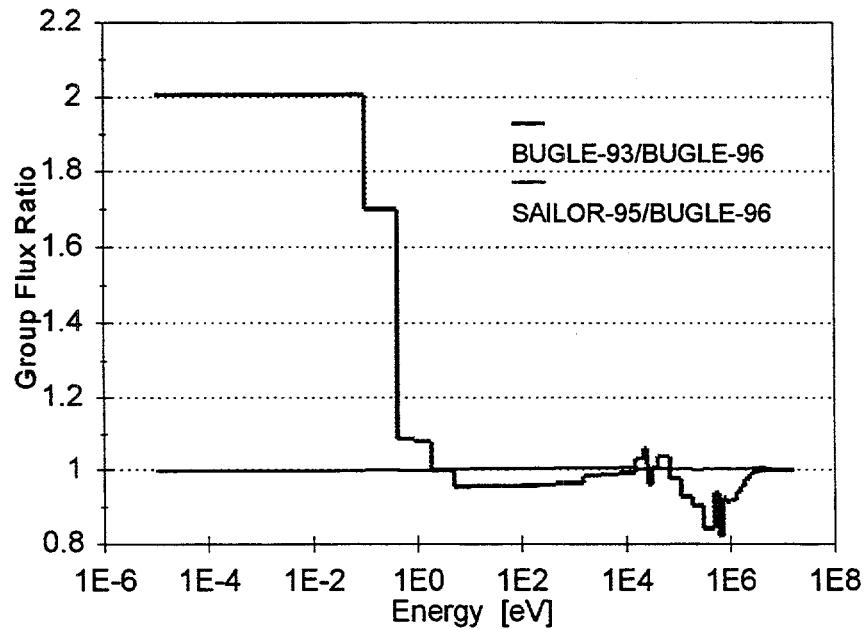

Fig. B.4 Comparison of multigroup neutron spectra, calculated with different cross-section libraries, at the position of cavity dosimeters (0°azimuth, core midplane, at the radius of 238.02 cm from core vertical axis)

1. REPORT NUMBER
(Assigned by NRC, Add Vol., Supp., Rev., and Addendum Numbers, if any.)

NUREG/CR-6453
ORNL/TM-13204

2. TITLE AND SUBTITLE

H. B. Robinson-2 Pressure Vessel Benchmark

3. DATE REPORT PUBLISHED

MONTH	YEAR
February	1998

4. FIN OR GRANT NUMBER
W6164

5. AUTHOR(S)

I. Remec, F. B. K. Kam

6. TYPE OF REPORT

7. PERIOD COVERED *(Inclusive Dates)*

8. PERFORMING ORGANIZATION – NAME AND ADDRESS *(If NRC, provide Division, Office or Region, U.S. Nuclear Regulatory Commission, and mailing address; if contractor, provide name and mailing address.)*

Oak Ridge National Laboratory
Oak Ridge, TN 37831-6363

9. SPONSORING ORGANIZATION – NAME AND ADDRESS *(If NRC, type "Same as above"; if contractor, provide NRC Division, Office or Region, U.S. Nuclear Regulatory Commission, and mailing address.)*

Division of Engineering Technology
Office of Nuclear Regulatory Research
U.S. Nuclear Regulatory Commission
Washington, D.C. 20555-0001

10. SUPPLEMENTARY NOTES
C. J. Fairbanks, NRC Project Manager

11. ABSTRACT *(200 words or less)*

The HBR-2 benchmark is specified and analyzed in this report. Analysis of the HBR-2 benchmark can be used as partial fulfillment of the requirements for the qualification of the methodology for calculating neutron fluence in pressure vessels, as required by the U.S. Nuclear Regulatory Commission Regulatory Guide DG-1053, "Calculational and Dosimetry Methods for Determining Pressure Vessel Neutron Fluence."

Section 1 of this report provides all the dimensions, material compositions, and neutron source data necessary for the analysis. The measured quantities, to be compared with the calculated values, are the specific activities of the neutron dosimeters, on both sides of the pressure vessel: in the surveillance capsule attached to the thermal shield and in the reactor cavity.

Section 2 describes the analysis of the HBR-2 benchmark with the computer code DORT and three ENDF/B-VI based multigroup libraries. The average ratio of the calculated-to-measured specific activities (C/M) for the six dosimeters in the surveillance capsule was 0.90 ± 0.04 for all three libraries. The average C/Ms for the cavity dosimeters (without neptunium dosimeter) were 0.89 ± 0.10, 0.91 ± 0.10, and 0.90 ± 0.09 for the BUGLE-93, SAILOR-95, and BUGLE-96 libraries, respectively.

12. KEY WORDS/DESCRIPTORS *(List words or phrases that will assist researchers in locating the report.)*

Neutron dosimetry
Neutron transport calculations
Qualification of the calculational methodology
Reactor pressure vessel
ENDF/B-VI
Benchmark
HBR-2

13. AVAILABILITY STATEMENT

Unlimited

14. SECURITY CLASSIFICATION

(This Page)

Unclassified

(This Report)

Unclassified

15. NUMBER OF PAGES

16. PRICE